LA-5121-MS
INFORMAL REPORT

C.3

A Reference Theta Pinch Reactor (RTPR)

A Study of a Pulsed High-Beta Fusion Reactor

Based on the Theta Pinch

los alamos
scientific laboratory
of the University of California
LOS ALAMOS, NEW MEXICO 87544

los alamos
scientific laboratory
of the University of California
LOS ALAMOS, NEW MEXICO 87544

A Reference Theta Pinch Reactor (RTPR)

A Study of a Pulsed High-Beta Fusion Reactor

Based on the Theta Pinch

by

S. C. Burnett
W. R. Ellis
T. A. Oliphant
F. L. Ribe

i

A REFERENCE THETA PINCH REACTOR (RTPR):

A STUDY OF A PULSED HIGH-BETA FUSION REACTOR BASED ON THE THETA PINCH

TABLE OF CONTENTS   PAGE

A REFERENCE THETA PINCH REACTOR (RTPR):

A STUDY OF A PULSED HIGH-BETA FUSION REACTOR BASED ON THE THETA PINCH

by

S. C. Burnett, W. R. Ellis, T. A. Oliphant, and F. L. Ribe

ABSTRACT

A design study of a pulsed high-beta θ-pinch reactor is presented. In the reference design developed here, the reactor generates 1.8 GWe with a duty factor chosen to limit the first wall nuclear power loading to 3.5 MW/m^2. Magnetic energy is switched reversibly into the compression coil from a cryogenic magnetic energy store situated outside the reactor core. The compression coil is protected from excessive nuclear radiation and heating by a portion of the neutron-moderating, tritium-breeding blanket. The blanket, in its present configuration, operates at a temperature of 800° C and has a breeding ratio of about 1.12. Flushing of He^4 and refueling between burning pulses is accomplished by flowing D-T gas through the discharge chamber. Some advantages of pulsed systems with respect to steady-state systems are discussed. Energy flow in the reactor is calculated, and it is shown that the circulating power fraction for the total system is approximately 10%.

I. INTRODUCTION

Previous feasibility studies[1,2,3] of pulsed θ-pinch reactors have dealt with systems in which a single-turn coil furnished both the implosion heating and adiabatic compression fields, as is the case in most present day θ-pinch experiments. The magnet coil was situated inside the neutron blanket and was gas-cooled. Such a system presents difficulties having to do with materials properties of the compression coil and with obtaining a sufficiently large excess of reactor energy output over the joule losses incurred in producing the magnetic field.

In this paper we describe a θ-pinch reactor based on a more sophisticated system, namely the staged θ pinch,[4,5,6] so called because it employs separate energy sources for the implosion-heating and adiabatic-compression stages. The implosion-heating coil is thin and liquid-metal-cooled. It is connected to a low-energy, high-voltage circuit whose cost and energy content are minor factors in the overall energy storage system. The energy in the magnetic compression field, which is preponderant, is furnished by a low voltage, multiturn coil which produces a more slowly rising magnetic field appropriate to adiabatic compression of the implosion-heated plasma. Such a coil is economical of joule electrical losses and leads to a satisfactory excess of reactor power output (low circulating power fraction). The compression coil is also of sufficient size to accommodate an inner neutron-moderating blanket.

The system which we describe below has not been optimized in a systematic way, and represents only one choice among many possible sets of parameters. In order to obtain specific results from the calculations, we have selected parameters which tend, in general, to minimize the core size. Some of the concepts and parameters presented here will doubtless not survive a detailed engineering study of the reactor system. Quantities which might change include plasma parameters (such as the starting temperature), the strength of the magnetic field, or construction materials, such as the

first wall insulator.

The purpose of this report, therefore, is not to give a detailed design study, but to present a self-consistent, introductory analysis of the θ-pinch reactor concept which includes the important physics. Improvements are expected as iterations are carried out. The relative ease with which a favorable energy balance is obtained in the present case is indicative of the basic reactor potential of the θ-pinch system.

II. BASIC PRINCIPLES OF THE STAGED θ-PINCH REACTOR

Figure 1 shows schematically the essential elements of a staged θ-pinch. In the shock-heating* stage a magnetic field B_s having a risetime of a few tens of nsec and a magnitude of a few tens of kG drives the implosion of a fully ionized plasma whose initial density is of the order of 10^{15} cm^{-3}. After the ion energy associated with the radially directed motion of the plasma implosion has been thermalized, the plasma assumes a temperature T_E, characteristic of equilibration of ions and electrons. The plasma radius $a_E = x_E b$, where b is the radius of the im-plosion-heating coil (Fig. 2). In Fig. 1 the dark-ly shaded areas represent magnetic field perpendic-ular to the plane of the figure. After a few μsec the adiabatic compression field (risetime a few msec and maximum value $B_0 \approx 100$ to 200 kG) is applied by energizing the compression coil (Fig. 1c). The arrow in Fig. 1c indicates the direction of magnetic energy flow into the system. The plasma is com-pressed to a smaller radius $x_0 b$ and its temperature is raised to a value $T_0 = 10$-20 keV. As the D-T plasma burns for several tens of msec, it produces 3.5-MeV α-particles which partially thermalize with the D-T ions and the electrons as the burned frac-tion of plasma increases to about 10% ; as a result the plasma is further heated. Given that the ratio β of plasma pressure to confining magnetic pressure, $B^2/8\pi$, is approximately unity, and assuming B to be approximately constant (B = B_0), the plasma expands against the magnetic field, doing work ΔW which is about 7% of the thermonuclear energy produced by

---

*The sort of shock heating we are discussing here can more properly be called "piston heating" or "implosion heating", since the magnetic field be-haves as a piston which ideally projects the ions forward at twice its velocity into a field-free region ahead of the sheath.

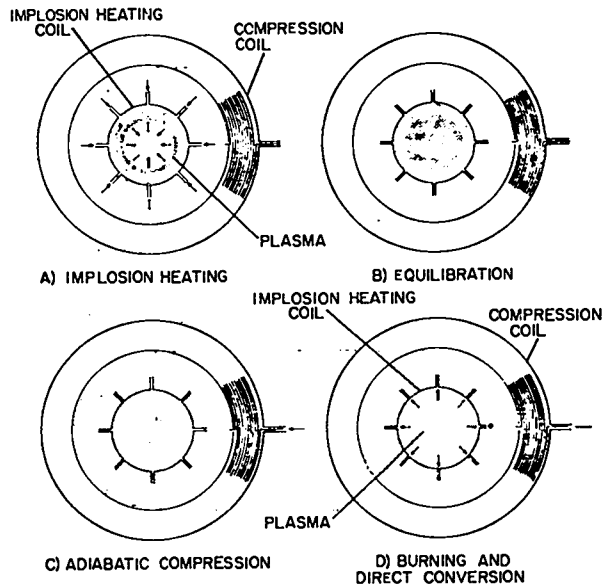Fig. 1. Illustrating plasma heating and burning in a staged θ-pinch reactor.
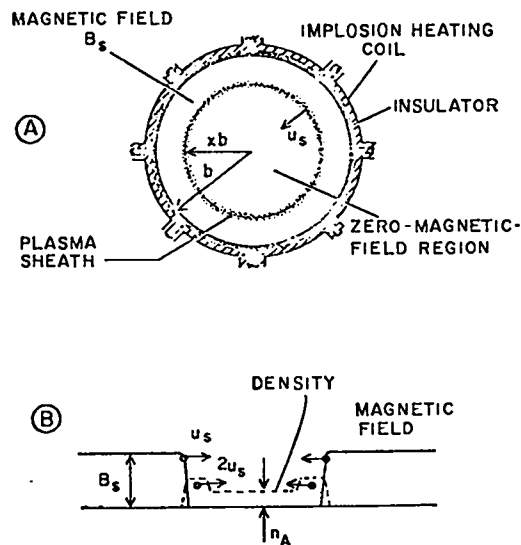

Fig. 2. Illustrating the processes involved in ideal implosion heating.

D-T fusion. This work produces an emf which forces magnetic energy out of the compression coil (cf. the arrow in Fig. 1d) and back into the compression mag-netic energy store. This high-β, α-particle heating and direct conversion has been treated in Refs. 1 and 7.

III. PLASMA HEATING

We will use the subscript "o" to refer to the plasma state at the end of the adiabatic compression phase, which is also taken as the start of the thermonuclear "burn". To obtain a plasma temperature kT_o after compression, for a given compression ratio $x_o = a_o/b$ (where a_o is the compressed plasma radius), we find from the adiabatic law

$$\frac{T_E}{T_o} = \left(\frac{a_o}{a_E}\right)^{4/f} \qquad (1)$$

where the subscript "E" refers to the equilibration state of the ions and electrons after the implosion heating and at the start of the compression. The quantity f is the number of degrees of freedom acquiring energy during the radial compression; f is generally between 2 and 3, depending on the density of the plasma and the time scale of the compression, and is related to the ratio of specific heats γ by

$$\gamma = \frac{f + 2}{f} \quad . \qquad (2)$$

Equation (1) specifies the amount of shock heating which is required in order to reach a starting temperature kT_o. To relate the required implosion-produced temperature T_E to quantities of practical interest such as filling pressure and applied implosion-heating voltage, we require a model of the shock heating process. A simple shock heating model has been described in Ref. (6) and is given in Appendix A.

A. Summary of Shock Heating Results

The shock heating requirements can be studied by taking as independent variables the first wall radius b, compression ratio x_o (= a_o/b), compression magnetic field B_o, and compressed plasma temperature kT_o at the start of the burn. Limiting consideration to the free-expansion case ($x'_{SH} = 0.76$), dropping all primes for convenience, and taking $\gamma = 5/3$ for the ratio of specific heats, we arrive at the following relations [equation (9), for example, is obtained by substituting (A-8), (A-12), (A-15), and (A-21) into (A-23)]:

$$B_S(kG) = B_o \left(\frac{x_o}{0.76}\right)^{1.66} \qquad (3)$$

$$P_A \text{ (mTorr)} = \frac{B_o^2 x_o^2}{(2.386)^2 \, kT_o} \qquad (4)$$

$$n_o \text{ (cm}^{-3}) = 1.24 \times 10^{13} \frac{B_o^2}{kT_o} \qquad (5)$$

$$kT_{SH} \text{ (keV)} = 2 \left(\frac{x_o}{0.76}\right)^{1.33} kT_o \qquad (6)$$

$$kT_E \text{(keV)} = \left(\frac{x_o}{0.76}\right)^{1.33} kT_o \qquad (7)$$

$$u_s \text{ (cm/}\mu\text{sec)} = 18.2 \left(\frac{x_o}{0.76}\right)^{.665} (kT_o)^{1/2} \qquad (8)$$

$$V_s \text{ (kV)} = 1.54 \, b \, x_o^{7/3} \, B_o (kT_o)^{1/2} \qquad (9)$$

$$E_\theta \text{ (kV/cm)} = \frac{V_s}{2\pi b} = 0.245 \, x_o^{7/3} \, B_o (kT_o)^{1/2} \qquad (10)$$

In all of the above equations B_o is in kG, kT_o is in keV, and b is in cm. The quantity B_s is the magnetic field required for implosion heating, P_A is the ambient filling pressure at 300°K in mTorr, n_o is the particle density after compression, kT_{SH} is the ion temperature imparted by the shock (before equilibration), kT_E is the ion and electron temperature after equilibration, u_s is the sheath (piston) velocity, V_s is the back emf induced around the coil, and E_θ is the azimuthal electric field at the insulating wall.

The parameters x_o, B_o, and b have been varied to determine the implosion heating requirements for various starting temperatures kT_o. Figure 3 illustrates the effect of varying x_o between 0.25 and 0.30 for b = 20 cm, B_o = 150 kG, and kT_o in the range 5 to 22.5 keV.

IV. SCALING LAWS FOR THERMONUCLEAR POWER PRODUCTION

We consider the thermonuclear burn to begin when the compression field reaches its final value B_o. Each neutron produced from D-T fusion is assumed to carry an energy $Q_n = 18.9$ MeV = 2.0 $\times 10^{-12}$ J.[*] For a plasma of radius a and plasma

---

[*] Q_n = 14.1 MeV kinetic birth energy, plus 4.8 MeV from the $Li^6(n,\alpha)T$ reaction in the blanket.
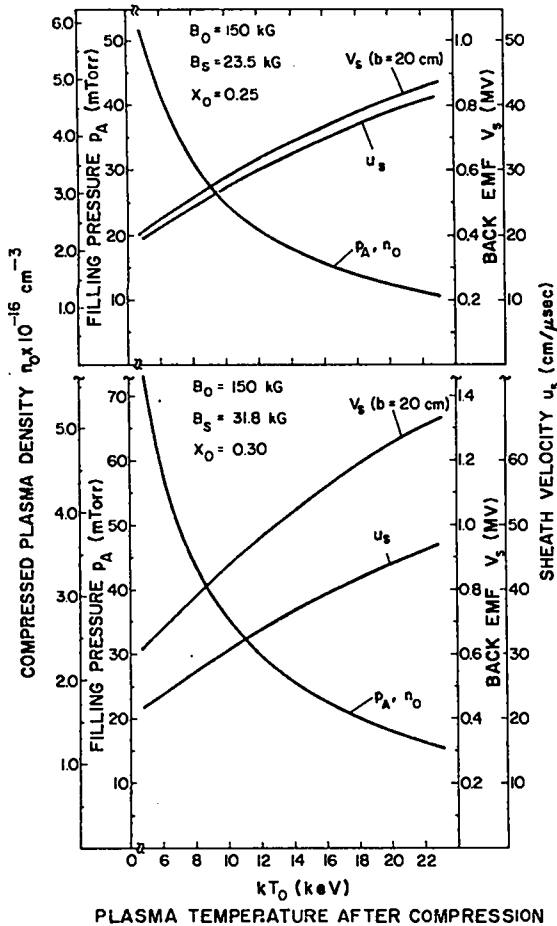
Fig. 3. Plasma back EMF, sheath velocity, filling
pressure, and compressed plasma density
versus starting D-T plasma temperature for
a 20 cm wall radius.

density n ($n_D = n_T = \frac{n}{2}$), the instantaneous thermo-
nuclear power per unit length produced in the lith-
ium blanket is

$$P_n = (\pi/4)a^2 n^2 Q_n \overline{\sigma v} \qquad (11)$$

where $\overline{\sigma v}$ is the Maxwell-averaged D-T cross section.
If we express B_o in kG, then before appreciable
burnup occurs, pressure balance at $\beta = 1$ requires,
from Eq. (5),

$$n_o kT_o = 1.24 \times 10^{13} B_o^2 \qquad (cm^{-3} \text{ keV}).$$

Substituting into (11) we obtain

$$P_n = 1.94 \times 10^{6} B_o^4 a^2 Q_n \overline{\sigma v}/(kT_o)^2 \qquad (MW/m) \quad (12)$$

for a in cm and B_o in kG, where the density does not
appear explicitly. The quantity $Q_n \overline{\sigma v}/(kT_o)^2 = 2.2$
$\times 10^{-14}$ cm^3/keV-sec for $kT_o = 15$ keV. Its value at
other temperatures is tabulated in Ref. 1.

V. PARAMETER SELECTION FOR THE REFERENCE THETA-
PINCH REACTOR (RTPR)

According to Eq.(11) one would like to have the
plasma density n_o as large as possible in order to
maximize reactor power output. This is equivalent
to having B_o as large as possible, since power pro-
duction scales as B_o^4 whereas joule losses scale as
B_o^2. In practice B_o will probably be limited to the
range 100-200 kG by the strength of materials (200
kG produces a pressure of 24,000 lb/in^2 on the com-
pression coil). In this reference design we shall
take $B_o = 150$ kG. For kT_o between 10 and 20 keV,
this fixes n_o between 1.4 and 2.8 x 10^{16} cm^{-3}, the
range encountered in present day θ-pinch experiments.

The scaling laws for plasma heating are sum-
marized in Eqs. (3)-(10). It is seen that the com-
pression ratio x_o should be kept as small as possi-
ble, consistent with anticipated wall stabilization
requirements, in order to minimize the necessary
implosion heating. Calculations show that a reas-
onable toroidal aspect ratio R/a, and hence plant
size, can be obtained for $x_o = 0.30$, while keeping
the starting number density,or pressure,and plasma
back emf V_s within reasonable limits. The filling
pressure can be reduced, which aids implosion heat-
ing, by achieving pressure balance with high initial
temperature as opposed to particle density. We
therefore choose $kT_o = 15$ keV for the Reference
Theta Pinch Reactor, which gives $n_o = 1.86 \times 10^{16}$
cm^{-3}. The wall radius b is selected on the basis
of implosion heating considerations and calcula-
tions of the overall energy balance for the RTPR
for various assumed blanket geometries. The choice
of b = 30 cm is found to give a satisfactory overall
energy balance and tritium breeding ratio in the
blanket.

These quantities specify the RTPR plasma at
the start of the burn, as shown in Fig. 4. The
dotted line gives the values corresponding to a
starting temperature of 15 keV. The parameters for
the start of the thermonuclear burn are listed in
Table I.

TABLE I

RTPR – Some Parameters at Start of Burn

Symbol	Definition	Value	
B_o	Compression field	150	kG
x_o	Compression ratio (a_o/b)	0.30	
b	Radius of shock heating coil	30	cm
kT_o	Electron and ion temperature at start of burn	15	keV
a_o	Plasma radius at start of burn	9	cm
kT_{SH}	Shock temperature of ions (before equilibration)	8.7	keV
kT_E	Electron and ion temperature (after equilibration)	4.35	keV
B_s	Implosion heating field	31.8	kG
u_s	Implosion velocity	38	cm/μsec
V_s	Plasma back emf	1.62	MV
E_θ	Implosion heating electric field	8.6	kV/cm
P_A	Ambient filling pressure	23.7	mTorr
n_o	Ion density ($n_D = n_T = \dfrac{n_o}{2}$) at start of burn	1.86×10^{16}cm^{-3}	
β	Ratio of plasma to magnetic pressure	~1	
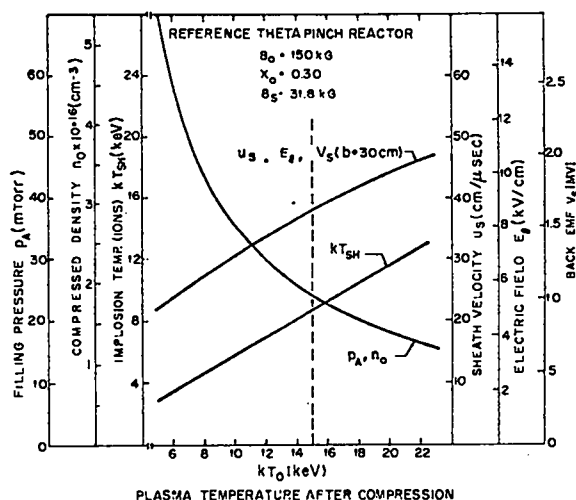
Fig. 4.   Summary of heating parameters for the Reference Theta Pinch Reactor (wall radius = 30 cm).

VI. TIME HISTORY OF THE THERMONUCLEAR CYCLE

The Reference Theta Pinch Reactor is designed for repetitive pulsed operation. Figure 5 shows schematically the main events in the cyclic time history. The implosion field B_s is applied suddenly and sustained for a time sufficient for the equilibrated plasma of temperature T_E to be "picked up" by the compression field. The rise time of the compression field B_o is taken as 10 msec, and the compression field is held constant during the burn time τ of 100 msec. The plasma at the start of the burn is designated as state "o". The plasma at the end of the burn is designated as state "f". At the end of the burn the plasma contains approximately 11% helium ions. The magnetic field is then relaxed to some lower value which allows expansion of the plasma column radially to the vicinity of the wall and extinguishes the burn. Neutral gas flows between the wall and the plasma boundary, removing heat from the column and neutralizing the plasma.
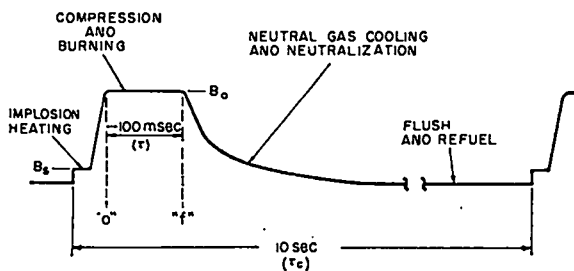
Fig. 5. Schematic of magnetic field waveform.

During the remainder of the cycle "off time," the plasma and hot gas are flushed out of the system and replaced by fresh plasma with negligible helium content. The refueling cycle is described in more detail in Sec. IX.

The ratio ξ of the cycle time τ_c to the burning time τ determines the average thermal power loading P_W on the reactor first wall, which is the implosion heating coil in the present case. The cycle time $\tau_c = 10$ sec is chosen to limit P_W to 3.5 MW/m^2 (350 W/cm^2) in the RTPR, giving a reactor duty factor (ξ^{-1}) of 1%. The instantaneous loading during the burning pulse exceeds P_W by about two orders of magnitude. Heat transfer will not balance heat deposition during the burning pulse, and care must be taken to design for reasonable temperature rises and thermal gradients in the first-wall and blanket materials. During the off-time of the reactor cycle, heat transfer from liquid lithium at the first wall and in the blanket reduces the material temperatures to their ambient values. The same choice of duty factor which places P_W in the 3.5 MW/m^2 range also leads to reasonable values of heat-transfer coefficient, i.e., to reasonable flow conditions for the lithium.

An important feature of the pulsed reactor with a small duty factor is that during heat transfer the lithium need not be pumped across the magnetic field. Thus it does not incur electromagnetic pumping losses, as in a steady-state reactor. Also, during heat transfer, the lithium flow is not along magnetic lines, since the field is absent. Thus the flow retains its turbulent character, which is prevented in the steady-field case. This allows the field-free heat-transfer coefficient in a pulsed reactor to be an order of magnitude higher than is possible in steady state systems.

VII. PULSED MAGNETIC ENERGY STORAGE FOR ADIABATIC COMPRESSION

Reversible magnetic energy transfer and storage systems appropriate to the compression phase of pulsed, high-beta reactors have been studied in detail by K. Thomassen (Ref. 11). A summary is given here of the torque-free system designed for the RTPR.

The cryogenic magnetic energy source must supply the magnetic compression energy in pulses of ~ 10 msec risetime and ~ 100 msec duration, separated by times of ~ 10 seconds. A circuit which would accomplish this pulsed energy transfer in a reversible manner is shown in Fig. 6. Large amounts of magnetic energy (~ 315-MJ per meter of reactor length) are stored in the cryogenic storage system, which in this example consists of modules containing three nested spherical coils and a transformer.

The two inner spherical coils of a module (each of which alone produces a uniform field in its interior and an exterior dipole field) have their magnetic fields at right angles, so are in quadrature, or uncoupled. This pair rotates inside the outer coil, alternately aligning the outer coil with one or the other of the inner coils. The coupling of the two inner coils to the outer coil varies as sin θ and cos θ respectively, and if the radii of the two inner coils are properly chosen, the total system energy is independent of the inner coils' position (θ). Thus, the rotor can be turned with zero torque in theory. This torque-free system was first proposed by P. F. Smith[12] of the Rutherford Laboratory, and further developed by Smith and Lewin[13] and Thomassen.[11]

By rotating the inner coils from $\theta = -90°$ to $\theta = +90°$ the currents in the various circuits are those shown in Fig. 7. The energy to the load increases as sin$^2\theta$ to the final value. The circuit theory for this system is given in Appendix B, where we show that more than 60% of the energy stored in the system can be transferred to and recovered from the load.

In the present design[11] each module transfers 140-MJ (of 225 MJ) to the load, and will drive ~2/3 of a meter. The module parameters are listed in Table II. The design requires only that one choose the transferred energy, the magnetic field strength in coil 1 (acting alone), and the current density in the superconductor. From these follow the coil

(a)

(b)
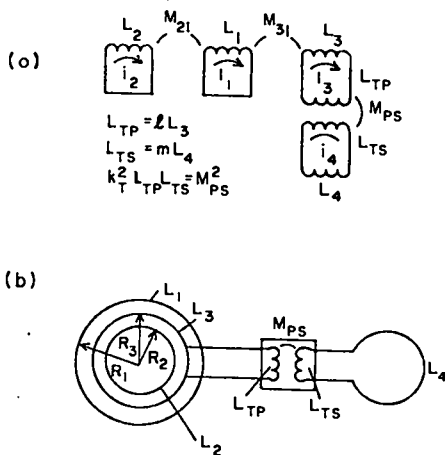
Fig. 6. (a): Circuit model of the energy transfer
system in (b). Coils 2 and 3 are mechani-
cally linked and electrically in quadra-
ture. Energy is coupled out of Coil 3
through the energy storage transformer M_{PS}
to load Coil 4.

$$L_{TP} = \ell L_3$$
$$L_{TS} = m L_4$$
$$k_T^2 L_{TP} L_{TS} = M_{PS}^2$$

Fig. 7. Current variation with θ for the circuit
of Fig. 6 (a).
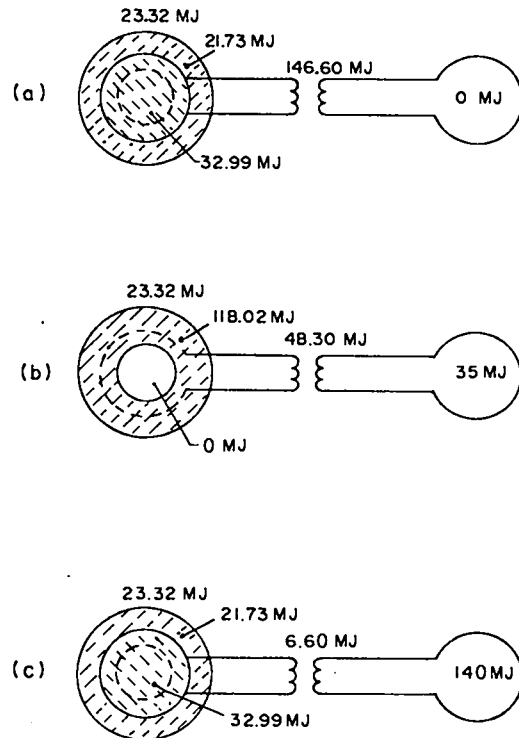
Fig. 8. Distribution of stored energy for: (a)
$\theta = -90°$ (b) $\theta = 0°$ (c) $\theta = 90°$.

radii, number of ampere-turns, superconductor volume
and mass and currents. The amount of energy stored
in various regions at the initial ($\theta = -90°$), in-
termediate ($\theta = 0°$) and final ($\theta = 90°$) stages is
shown in Fig. 8. To recover the energy one simply
rotates the coils back to their initial positions.

The advantages of this system are the high en-
ergy transfer ratio and the ability to synthesize
an arbitrary current pulse in the load coil. Also,
the system is stationary between pulses so the av-
erage superconducting a.c. losses should be small.
The only disadvantage is that considerable inertial
energy must be expended (55 MJ) to raise the field
in 10 msec. This inertial energy scales as
$W^{4/3} B^{-5/3} J^{-1}$, with W = energy, B = field strength,
and J = current density. Developments in super-
conducting technology will obviously help to alle-
viate this difficulty. With a superconductor cap-
able of 10^5 A/cm^2 at 100 kG the inertial energy
will be only 10% of the stored energy, so that the
internal energy can then be used to supply the in-
ertial requirement. The method has been described
by Smith and Lewin.[13]

VIII. FUEL BURNUP AND DIRECT ENERGY CONVERSION

The scaling laws for power production P_n in
Sec. IV are accurate for a plasma of unvarying
properties, i.e., for negligible D-T burnup. As
the burn proceeds however, 3.52 MeV alpha (α) par-
ticles are produced which constitute an energy
source in the plasma column. The large energy depo-
sition in the plasma makes the thermonuclear burn
in a θ pinch a non-linear, dynamic process which
requires computer solution for realistic answers.

TABLE II - Design Parameters for a Superconducting Energy Transfer Module

Symbol	Definition	Value
k_T^2	coupling coefficient	0.98
k_m^2	coupling coefficient	0.9
η	transfer efficiency	62.3 %
B_{o1}	field strength of coil 1	60 kG
W_{MS}	total magnetic energy stored	225 MJ
W_{MT}	energy transferred to load	140 MJ
R_1	coil radius	1.47 m
R_2	coil radius	1.17 m
R_3	coil radius	1.42 m
$N_1 I_1$	ampere turns	2.10×10^7 A
$N_2 I_2$	ampere turns	1.68×10^7 A
$N_3 I_3$	ampere turns	1.14×10^7 A
J	current density	10^5 A/cm^2
δ_1	coil thickness	4.56 mm
δ_2	coil thickness	4.56 mm
δ_3	coil thickness	2.56 mm
V_1	superconductor volume	12.4×10^4 cm^3
V_2	superconductor volume	7.85×10^4 cm^3
V_3	superconductor volume	6.47×10^4 cm^3
$I_{\omega 1}$	moment of inertia	1710 kg m^2
$I_{\omega 2}$	moment of inertia	554 kg m^2
$I_{\omega 3}$	moment of inertia	669 kg m^2

We can get an estimate of the α-particle heating effect by calculating the pressure increase in the plasma column which would occur if expansion were prevented (for example, by increasing the external field B_o). After the burn the final particle pressure would be given by

$$P_f = P_o + \frac{2}{3} n_{\alpha f} E_{\alpha b} \qquad (13)$$

where

$$P_o = 2n_o kT_o \qquad (14)$$

is the particle pressure at the start of the burn, $n_{\alpha f}$ is the final number density of α-particles, and $E_{\alpha b} = 3.52$ MeV is the α-particle birth energy.

The fractional burnup of fuel ions is given by

$$f_B = \frac{2n_{\alpha f}}{n_f + 2n_{\alpha f}} \qquad (15)$$

where n_f is the final ion density. In the case of zero expansion,

$$n_f = n_o - 2n_{\alpha f} . \qquad (16)$$

(Two ions are involved in the production of a single α particle). Combining (13) – (16) yields the pressure ratio as

$$\frac{P_f}{P_o} = 1 + \frac{f_B E_{\alpha b}}{6 \ kT_o} \qquad (17)$$

$$= 1 + 39.1 \ f_B \qquad (18)$$

for $E_{\alpha b}$ = 3.52 MeV and kT_o = 15 keV. Equation (18) is plotted in Fig. 9. The internal pressure would increase nearly five-fold for a 10% fuel burnup, and forty-fold for complete burnup. This pressure is available to do work against the magnetic field.

For the case of a β = 1 plasma and a constant external field B_o, the α-particle pressure will cause the plasma to expand from initial radius a_o to final radius a_f, doing an amount of work

$$\Delta W = \pi \ (B_o^2/8\pi) \ (a_f^2 - a_o^2). \qquad (19)$$

This work is available to the driving magnetic energy source at essentially 100% efficiency. Together with the regulation of the burn which it entails, the plasma expansion constitutes a major advantage of the θ-pinch reactor over low β systems.

A. A Computer Program for Burnup.

A program[7] has been written for the CDC 7600 which computes the effects of burnup and α-particle production on the plasma parameters, net power production, bremsstrahlung losses, etc., as a function of the burning time. The procedure involves numerical solution of the Fokker–Planck equation. The various particle distribution functions are obtained from which the physical quantities of interest such as the number densities and temperatures for the
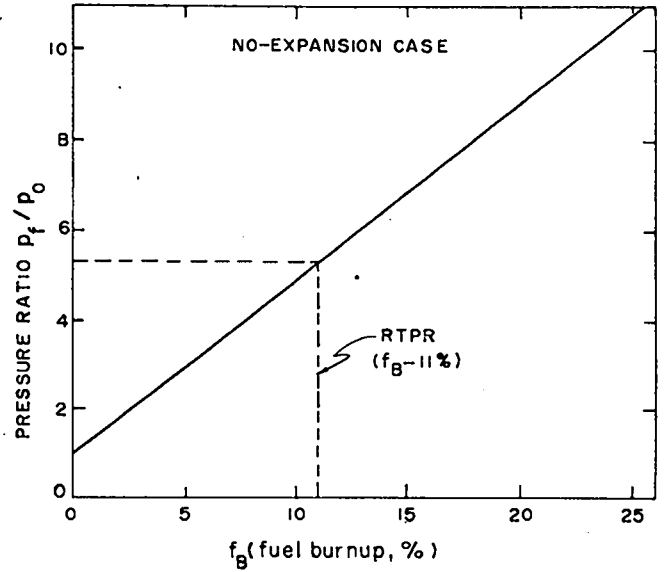
Fig. 9. Pressure increase as a function of fuel burnup for the case when no plasma expansion is allowed.

plasma electrons, ions, and α particles, the amount of direct conversion work ΔW, etc., are calculated. The quantity $\Delta W/P_n \tau$, calculated entirely from the Fokker–Planck code, is found to have a value 0.07 (to within 1%) during the entire 100 msec burn. The quantity P_n is calculated in its time dependent form from Eq. (11).

Figure 10 shows the variation of the particle temperatures and densities for the RTPR as a function of the burn time. The large initial reaction rate produces a rapid buildup of α particles. The α-particle partial pressure causes the plasma column to expand. Due essentially to adiabatic decompression, the ion and electron temperatures drop during the first few msec of the burn, before appreciable energy transfer occurs between the hot α's and the plasma particles. As the burn proceeds, the α particles preferentially heat the electrons, whose temperature always leads the ion temperature, even though the electrons undergo bremsstrahlung radiation cooling (an effect included in the code).

As burnup progresses, the plasma expands and the density decreases monotonically in time. After the start of the burn the electron density is always greater than the fuel ion density n by an amount

$$n_e = n + 2n_\alpha \qquad (20)$$

9
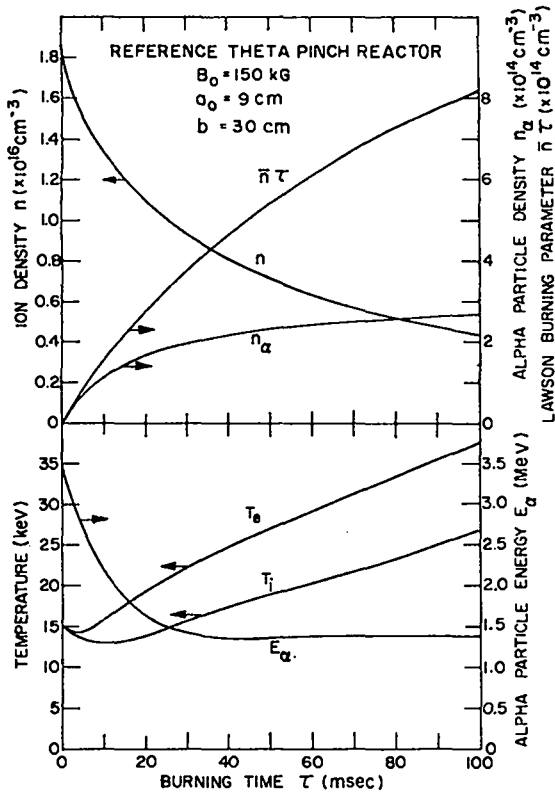
Fig. 10. Computed electron and ion temperatures, alpha particle energy, ion density, alpha particle density, and integrated Lawson parameter as a function of the burn time τ.

Fig. 11. Computed plasma radius, neutron energy production, and bremsstrahlung energy production as a function of the burn time τ.

since the total number of electrons is not changed during burnup. The ion density variation leads to a non-linear variation of the integrated Lawson parameter $\bar{n}\tau$ as a function of the burn time (Fig. 10). The final value for the RTPR after 100 msec is ~ 8×10^{14} cm^{-3} sec, leading to a satisfactory energy surplus for the overall reactor system.

Figure 11 shows the effect of plasma expansion on thermonuclear power production, bremsstrahlung, and plasma radius. The quantity

$$\frac{W_n}{W_{no}} = \frac{\int_o^\tau P_n(t)dt}{P_{no}\tau} \qquad (21)$$

compares the Fokker-Planck result for the thermonuclear energy per unit length, to that calculated from (12) assuming initial conditions a_o and kT_o and multiplying by the burn time τ (i.e. no burnup is considered in Eq.(12)). Figure 11 also gives the quantity W_{BR}/W_{BRo}, which compares the Fokker-Planck result for bremsstrahlung radiation loss to the analytic calculation[1] based on initial conditions:

$$W_{BRo} = 1.72 \times 10^{-34} a_o^2 n_o^2 (kT_o)^{1/2}\tau \quad MJ/m \quad (22)$$

for kT_o in keV.

Table III summarizes some plasma conditions before and after the 100 msec burn.

IX. GAS DYNAMIC FLUSHING AND REFUELING

An attractive feature of a pulsed fusion reactor is the possibility of removing the alpha-particle "ash" resulting form the deuterium-tritium (D-T)

TABLE III

RTPR - Plasma Parameters During Burn ($B_o = B_f = 150$ kG)

Symbol	Definition	Value
a_o	Initial plasma radius	9.0 cm
a_f	Final plasma radius	17.33 cm
kT_o	Initial temperature (ions & electrons)	15 keV
kT_{if}	Final ion temperature	26.7 keV
kT_{ef}	Final electron temperature	37.5 keV
$E_{\alpha f}$	Final α-particle mean energy	1.39 MeV
n_o	Initial particle density (ion and electron)	1.86×10^{16} cm^{-3}
n_f	Final ion density	4.37×10^{15} cm^{-3}
n_{ef}	Final electron density	4.91×10^{15} cm^{-3}
$n_{\alpha f}$	Final α-particle density	2.72×10^{14} cm^{-3}
$\bar{n}\tau$	Integrated Lawson parameter	8×10^{14} cm^{-3} sec
f_B	Fractional fuel burnup	~11%
τ_c	Cycle time	10 sec
τ	Burn time	0.10 sec
ξ^{-1}	Duty factor	1%

fuel burnup and injecting new fuel by D-T gas flow between burning pulses. Thus, no divertor is required, as in the case of a steady-state toroidal reactor. A blanket of gas between the hot central plasma and the first wall can be used to cool, neutralize, and replace the partially burned D-T plasma. Sputtering problems are alleviated, since heat transfer to the wall, which would otherwise occur by energetic ions, should now occur primarily by means of neutral atom thermal conduction and to a lesser extent by ultraviolet and visible radiation.

A. Initial Conditions.

The initial conditions for the flushing calcu-

lation are taken from the final conditions of the plasma burn as given in Table III. Thus $n_e \approx 4.91 \times 10^{15}$ cm^{-3}, $n = 4.37 \times 10^{15}$ cm^{-3}, $n_{\alpha} \approx 2.72 \times 10^{14}$ cm^{-3}, $E_{\alpha} = 1.39$ MeV, $kT_e = 37.5$ keV, $kT_i = 26.7$ keV, and $a = 17.33$ cm. Since energy equipartition among the alphas, ions, and electrons takes place in a time short compared to the flushing time (which is of the order of 10 sec), it may be assumed to take place instantaneously at the beginning of the flushing operation. The equilibrium plasma temperature at $a_f = 17.33$ cm is then given by:

$$kT_f^* = \frac{(n_\alpha E_\alpha)_f + \frac{3}{2}(n_f \, kT_{1f} + n_{ef} kT_{ef})}{\frac{3}{2}(n_{\alpha f} + n_f + n_{ef})} \qquad (23)$$

$$= 59.2 \text{ keV}.$$

The total energy content of the plasma (including α-particles) is given by

$$W_p^* = \frac{3}{2}(B_o^2/8\pi)\,\pi a_f^2$$

$$= 1.3 \times 10^5 \text{ J/cm}$$

of reactor length. If this heat is extracted by thermal conduction to the walls through an intervening neutral gas layer, the total heat delivered to the first wall is 670 j/cm^2. If this heat is extracted in ~10 sec, then the average thermal wall loading from the plasma after-heat is ~67 W/cm^2.

The plasma burn is quenched prior to the flushing operation by allowing the plasma to expand adiabatically to the vicinity of the wall, dropping both the temperature and density. If the plasma radius increases from 17.33 cm to, say, 25 cm, still maintaining a $\beta = 1$ plasma, the temperature drops from 59.2 keV to 36.4 keV, the density drops by a factor of 2.08, and the reaction rate decreases correspondingly. The expansion is accomplished by decreasing the magnetic field from 150 to 81 kG.

B. Model of Plasma Cooling.

We now assume that further heat production in the plasma is negligible and compute the plasma temperature profile, ionization profile, and heat transfer to the wall on the following model. Cool (800 °C) D-T fuel is assumed to flow into the annular region between the plasma and the wall in a time short compared to the cooling time, and the neutral atom density is taken to be 1.67×10^{15} cm^{-3}, i.e., the starting density required for the next pulse. The magnetic field is programmed to decrease in some manner with time. In the case discussed here, B(t) is chosen so that the magnetic field interface remains stationary at a = 25 cm as the plasma cools.

Collisions are assumed to maintain a common temperature for ions, neutrals, and electrons. The wall is maintained isothermally at 800 °C (0.07 ev),

and the gas layer immediately adjacent is thus almost totally neutral. Adjacent to the hot plasma the gas layer becomes completely ionized. The ionization profile, and hence the heat transfer mechanism, is strongly radius-dependent, and requires a fine mesh for the computations. Ion-neutral recombination coefficients are taken from Bates, Kingston, and McWhirter.[14]

When the hot plasma contacts the cool gas layer, a rapid transfer of heat takes place out of the plasma, ionizing the neutrals and very quickly establishing a quasi-steady temperature profile. Thermal conductivity in a partially ionized gas is a strong function of the degree of ionization, which depends on the local temperature and density. These in turn depend on the heat conduction, so that a self-consistent problem must be solved.

Although the magnetic field interface and wall radius are fixed, there will be internal motion in the gas layer as a result of pressure gradients arising from the changing temperature profile as heat flows through the layer. The net effect of this motion is to shift some of the gas layer material closer to the wall, leaving a sparser density of ions just outside the magnetic field interface. As pointed out by Lehnert,[15] there will be a flow of ions and neutrals relative to each other driven by the separate pressure gradients. However, this flow is strongly limited by $\vec{v} \cdot \nabla \vec{v}$ terms in the momentum equations and will have little effect on the overall temperature profiles.[16]

In the preliminary calculation presented in this section, the gas layer is assumed rigid so that this motion is ignored and pointwise pressure balance is not maintained within the layer. However, the qualitative features of thermal conduction and ionization rates, which are the most important physical phenomena, are still well represented. A fully self-consistent, hydrostatic pressure balance adjustment is being added to the computer program and the improved results will appear as a separate LA report in the near future along with a more detailed discussion of the flushing problem.

C. Computational Results.

Results are represented in Figs. 12 and 13 for the cooling model described above, wherein the magnetic field interface is held fixed at a = 25 cm. In this case the temperature gradient driving the
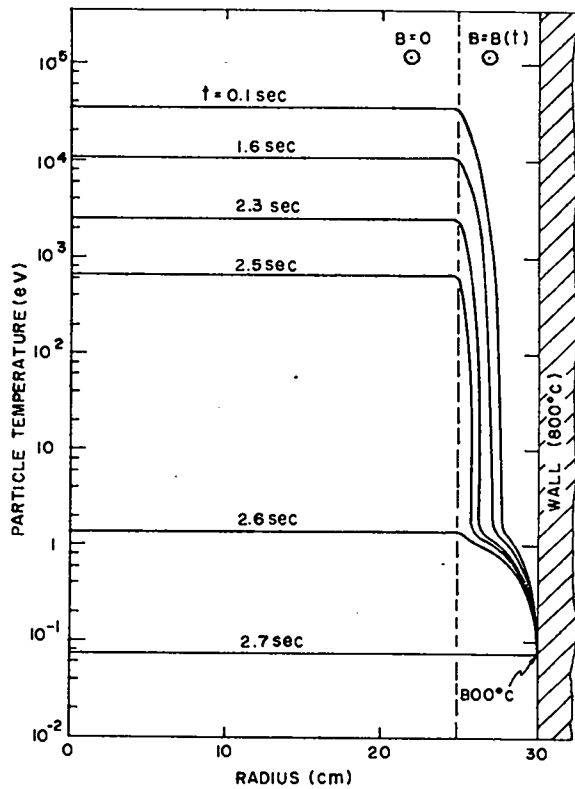
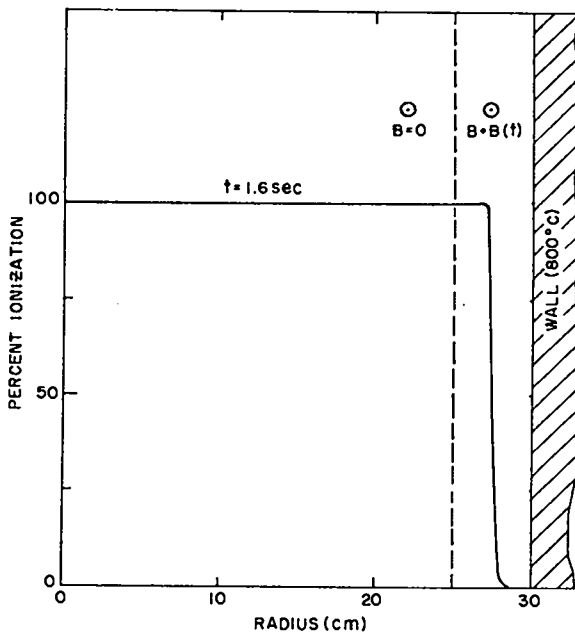Fig. 12. Computed curves of plasma temperature as a function of radius and time during the flushing cycle.

Fig. 13. Typical computed curve for ionization level vs radius (at t = 1.6 sec) in the flushing cycle.

heat flow is a function of time though the reduction of the upper (plasma) temperature. The heat is taken out of the plasma approximately linearly in time, with the plasma temperature falling to 10.3 keV in 1.6 sec. By 2.7 sec the temperature profile is flat, and the entire gas-filling has the uniform temperature of 800 °C. At this time mixing begins between the old gas and the new, and the now neutralized helium can be flushed out of the chamber in the remaining seven seconds or so of the cycle. The heat transfer rate to the wall can be increased, and the heat load reduced, by decreasing the amount of initial decompression to, say, 20 cm, if desired, since the width of the temperature gradient can be used to regulate the heat flow.

The "breaking point" or "foot" of the temperature profiles, which is a distinguishing feature, occurs at the transition from ion to neutral atom populations and reflects the fact that atom thermal conduction is much faster than ion thermal conduction, and requires a temperature gradient which is correspondingly orders of magnitude smaller. The time specified in Figs. 12 and 13 is counted from the start of the conduction problem, i.e. after adiabatic decompression, which is ~0.1 sec after the start of the cycle.

X. THE OVERALL REACTOR SYSTEM.

A schematic diagram of the overall reactor system[17,18] is shown in Fig. 14. The implosion heating coil with a number of radial transmission-line feeds (8 are shown) is surrounded by a Li-Be-C blanket which has three functions: (a) It absorbs all but a few percent of the 14-MeV neutron energy from the plasma, which the flowing lithium carries out to heat exchangers in the electrical generating plant. (b) It breeds tritium by means of the $Li^7(n,n´\alpha)T$ reaction for fast neutrons and the $Li^6(n,\alpha)T$ reaction for slow neutrons. (c) The high Reynolds-number flow of liquid lithium cools the first wall(implosion-heating coil).

Outside the inner blanket region is the multiturn compression coil which is energized by the slowly rising current (~10 kA per cm of its length) from the secondary of the cryogenic magnetic energy store. The compression coil consists of the coiled up parallel-sheet transmission lines which bring in the high voltage (V_s of Eq. (9)) to the feed slots
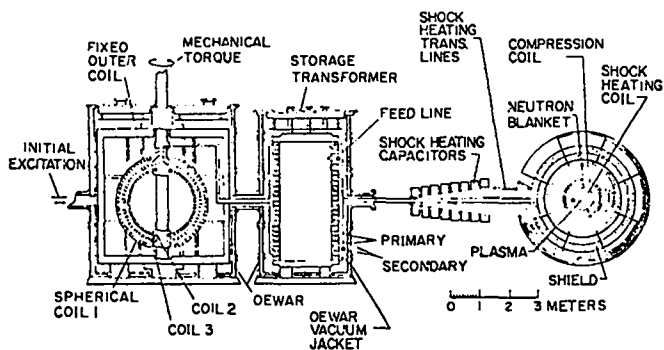
Fig. 14. Schematic cross section view of the RTPR. The reactor core and compression coil are shown on the right and the METS system is shown on the left.

of the implosion-heating coil. Each side of the horizontal feed of the secondary coil also serves as a ground plane for the high-voltage implosion-heating circuit (including crowbar capacitors for sustaining the implosion-heating field B_s). Each transmission line delivers a feed point voltage V_{fp} to one of the radial feed slots, where V_{fp} is of the order of V_s divided by the number of feed points. In the case of the RTPR, V_{fp} is approximately 50-kV for 32 feed slots. Eight feed slots are shown in Fig. 14 for the purposes of illustration. A discussion of possible circuitry for accomplishing this dual use of the coiled up transmission lines is given in Appendix C.

Outside the compression coil and its titanium coil backing is the remainder of the neutron blanket for "mopping-up" the last few percent of neutron energy and breeding the last few percent of tritium. Unlike the inner blanket, which would run at ~800 °C to provide high thermal efficiency of the generating plant, this portion of blanket could run substantially cooler. Surrounding the outer blanket is a radiation shield, and beyond the shield the radially emerging transmission lines are brought around to make contact with the secondary-coil current feeds and the high-voltage implosion-heating circuits. To the left are shown the cryogenic energy storage and transfer coils of Fig. 8 in their dewar.

XI. NEUTRONICS CALCULATIONS AND BLANKET DESIGN.

Neutron flux and reaction rate distributions

have been determined for the RTPR blanket model shown in Fig. 15. These spectral-spatial data have been analyzed to determine quantities of interest such as the breeding ratio, energy deposition, displacements per atom (dpa), helium production, and transmutation. The RTPR neutronic analysis given here is by Dudziak.[19] This work has evolved from previous neutronic studies by Bell.[20,21]

All neutronics transport calculations were performed with the DTF-IV discrete-ordinates code,[22] using S_4 quadrature in a one-dimensional cylindrical geometry. Cross-sections for the 9 materials composing the reactor blanket were 100-group, infinitely dilute, P_3 multigroup values processed from the ENDF-III data file[23] into the GAM-II energy structure.[24] A uniformly distributed volumetric source was placed in a plasma region with a 15-cm mean radius. At the outer surface of the mop-up blanket (r = 155 cm), a vacuum boundary condition was assumed. Adequacy of an S_4 - P_3 analysis to predict an integral quantity such as breeding ratio within ~2% (as compared to S_{12} - P_3) was shown previously for a CTR blanket benchmark.[25] Many studies, including one for a CTR benchmark,[26] have demonstrated the sufficiency of a P_3 truncation of scattering matrices, and of the uniform source assumption.

Because the θ-pinch reactor concept is not sensitive to neutron transport through the outer shield (i.e., no superconducting-coil magnet surrounds the reactor), the model ended at the "mop-up" blanket. This blanket provides a very minor contribution of 0.003 to the total breeding ratio of
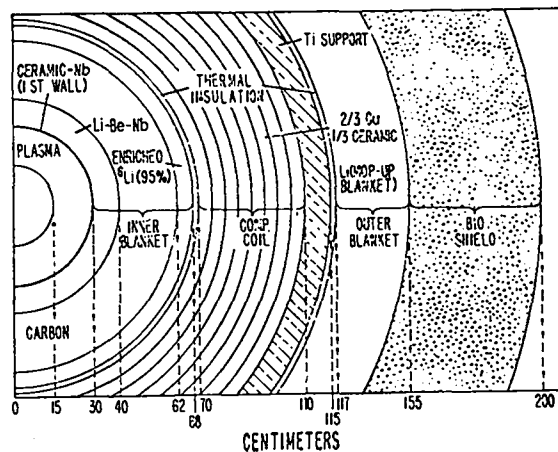

Fig. 15. Model of the RTPR blanket used for neutronics calculations.

1.07*, so it may well be replaced by shielding in future RTPR designs.

Approximately 43% of the breeding occurs in the first Li region (66^v/o Li, 25^v/o Be, 4^v/o Al$_2$O$_3$, 5^v/o Nb) and 27% in the graphite region (10^v/o Li, 86^v/o C, 2^v/o Nb, 2^v/o Al$_2$O$_3$), with the remainder in the 95^a/o enriched ^{6}Li region (92^v/o Li, 4^v/o Al$_2$O$_3$, and 4^v/o Nb). Atom number densities were calculated for a uniform blanket temperature of 800 °C, except for the graphite region (1000 °C), compression coil (20 °C), and mop-up blanket (500 °C).

The lithium in the outer, or mop-up, blanket need not circulate, but its assumed 500 °C temperature is high enough for the lithium to be molten and phase-stable, and low enough to be compatible with, if desired, a stainless steel casing (not shown) ahead of the shield.

As with all CTR concepts, radiation damage to the first wall is of major concern. Accordingly, helium-production and atom-displacement rates have been determined for the niobium structure, assuming a 3.5 MW/m^2 time-average wall loading. Values of 97 ppm He/yr and 59 dpa/yr were determined for the inner surface of the first wall. These compare with values of 94 ppm/yr and 74 dpa/yr for a reference ORNL tokamak reactor[27] at the same wall loading. Displacement damage, computed using recently available damage functions,[28] is approximately half that for structural materials of a typical experimental fast breeder reactor. However, possible synergistic effects of displacement damage and much higher He production in CTR's are still unknown.

Neutron heating in the Cu of the compression coil (67^v/o Cu, 33^v/o Al$_2$O$_3$) is of considerable importance because of heat removal requirements. Using multigroup kerma factors,[29] the neutron energy deposition in Cu was found to be representable as 0.1178 exp-[0.1243 (r-70)] W/cm^3, for 70 $\leq$ r $\leq$ 110. At an incident 14-MeV current on the first wall of 3.5 MW/m^2, total neutron heating in the Cu coil is ~310 W per cm of reactor length. Detailed spatial calculations of gamma-ray energy deposition are now in progress; however, total gamma heating in the

Cu coil has been approximated from Q-values as ~3.51 kW per cm, or ~0.155 W/cm^3 averaged over the coil volume and ten-second pulse cycle.**

The overall tritium breeding ratio is defined by

$$T = \frac{\dot{N}^+}{\dot{N}^-} \qquad (24)$$

where $\dot{N}^+$ is the rate of tritium production and $\dot{N}^-$ is the rate of tritium consumption. For the RTPR we use T = 1.1, and $\dot{N}^-$ ~200 g/day for a 10 sec cycle time and a reactor length of 350 m. The tritium doubling time is given by[30]

$$t_d = \frac{I_{ex\ min} + I_{B\ sat}}{\dot{N}^- (T - 1)} \quad , \qquad (25)$$

(neglecting radioactive decay), where $I_{ex\ min}$ is the minimum tritium inventory external to the blanket and is taken in the present case to be ten times the daily consumption, i.e., a total of 2000 g. The saturated blanket inventory is proportional to the breeding ratio and inversely proportional to the removal constant λ:

$$I_{B\ sat} = \frac{T\dot{N}^-}{\lambda} \quad . \qquad (26)$$

The mean residence time for tritium in the blanket is 1/λ days, e.g., λ = 10/day. Substituting the above values into (25) gives a tritium doubling time of 101 days for the RTPR, or about three and one-third months.

In summary the RTPR has an adequate breeding ratio, which has been conservatively calculated by ignoring resonance self-shielding in the structure. The "mop-up" blanket contributes little to the breeding, and may be eliminated in favor of slightly more Li within the inner blanket if necessary. Alternate design options desirable from a neutronics viewpoint are: (1) Replace the graphite with BeO, possibly eliminating Nb cladding; (2) Introduce Li in the Cu compression coil to reduce the

---

*Accounting for resonance self-shielding in Nb may raise the breeding ratio by about 5%. Similarly, addition of 10^v/o Li in the compression coil region increases the breeding ratio by 4%.

**Addition of Li to the compression coil will decrease the effective Q-value and thus nuclear heating, as well as enhancing breeding.

present loss of ~11% of the neutrons by capture in Cu; and (3) Substitute Mo for Nb in the structure whenever possible, but especially from the first wall through the graphite region.

Energy deposition in the Cu is low enough to allow reasonable cooling system parameters.

XII. JOULE LOSSES IN THE REACTOR CORE AND COMPRESSION COIL

A. Contribution to Joule Losses.

In Figs. 14, 15, and 16 we define the reactor core as that portion of the reactor inside the compression coil. In the presence of the rising and falling compression field there will be eddy-current losses in the conducting lithium and carbon of the blanket, as well as in the turns of the compression coil itself. By suitably subdividing the conductors, however, these eddy-current losses can be made arbitrarily small. In addition, the compression field must "soak" through the refractory metal wall of the shock-heating coil resulting in some joule loss from the currents induced in this process. Finally the current in the compression coil which produces the compression field (transport current, see below) will produce the equivalent of d.c. joule losses for the duration τ of the compression pulse. These losses reflect significantly into the energy balance of the reactor.

B. Joule Losses of the Transport Current.

The current in a pulsed solenoid has two components, as shown in Fig. 17A. The transport current j_T furnishes the magnetic field B in the coil bore according to Ampere's law $\nabla \times \vec{B} = 0.4 \pi \vec{j}$. The eddy current density j_E, arising from the time variation of magnetic field, forms closed paths in the windings and does not contribute to the magnetic field on axis. It is governed by Faraday's law of induction $\nabla \times \vec{E} = -10^{-8} \partial\vec{B}/\partial t$. These two components are illustrated in Fig. 17B and discussed in Appendix E.

The energy loss from transport current is the same as for d.c. current. Using Ampere's law, we have for the current density

$$j_T = B_o / 0.4 \pi \lambda \Delta R_c, \qquad (27)$$

where ΔR_c is the total compression coil thickness,
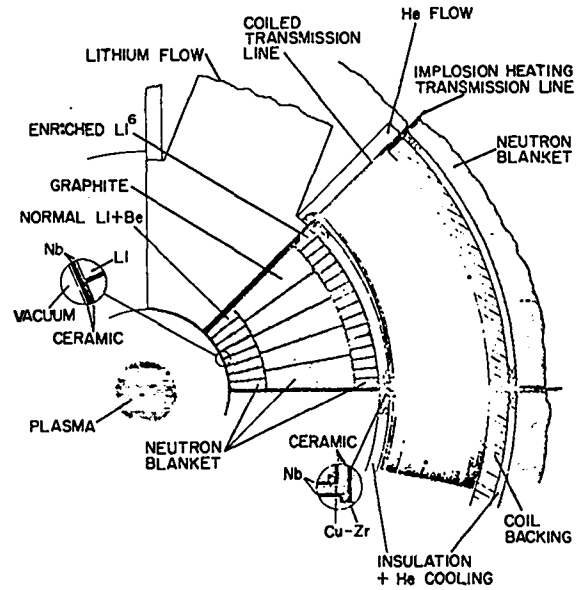
Fig. 16. Illustration of a possible reactor core and compression coil in the RTPR.

and λ is the volume filling factor of the conductor. If $\bar{R}_c$ is the mean coil radius,

$$\bar{R}_c = R_{co} + \frac{\Delta R_c}{2}, \qquad (28)$$

where R_{co} is the inside radius of the compression coil, the total joule energy loss per unit length W_T in the coil due to the driving (transport) current during a flat-topped pulse of duration τ and rise time τ_R (see Fig. 17c) is given by Eqs. (E-17) and (E-18) of Appendix E:

$$W_T = \frac{2\pi \bar{R}_c \, \eta \, B_o^2}{(0.4\pi)^2 \, \lambda \Delta R_c} \left(\tau + \frac{2}{3}\tau_R\right) \qquad (29)$$

$$= 4.0 \times 10^{-4} \frac{\bar{R}_c \, B_o^2 \, \eta}{\lambda \Delta R_c} \left(\tau + \frac{2}{3}\tau_R\right). \quad (MJ/m) \ (30)$$

where η is the coil resistivity. For the Reference Theta Pinch Reactor we have: $B_o = 150$ kG, $\bar{R}_c = 90$ cm, $\tau = 0.1$ sec, $\tau_R = 0.01$ sec, $\lambda = 0.7$, $\Delta R_c = 40$ cm, and $\eta_{Cu} = 1.7 \times 10^{-6}$ ohm-cm (for 20 °C copper), giving* $W_T = 5.24$ MJ/m.

*This analysis neglects joule losses in the compression coil incurred during flushing and refueling (Sec. IX). Power production during this phase of the cycle is also neglected when calculating the energy balance of the reactor (Sec.XIV).

LAYERS IN ΔR

$\overline{R}_c$

R_{co}

$B \cdot B(t)$ $B \cdot 0$

R_c^*

A

MAGNETIC FIELD

B_v

B_l

$B(t)$

B_l

x

τ_R τ_R

B_o

τ

CURRENT DENSITY

EDDY CURRENT
TRANSPORT
CURRENT

j_T

x

i_T

i_E

RADIAL DISTANCE

TIME

B   C

Fig. 17. A. Multiturn magnetic compression coil
             showing transport and eddy currents
             and the radii R_{co}, R_c^*, and $\overline{R}_c$.

       B. Radial distribution of magnetic field,
           transport current, and eddy current.

       C. Time variation of magnetic field,
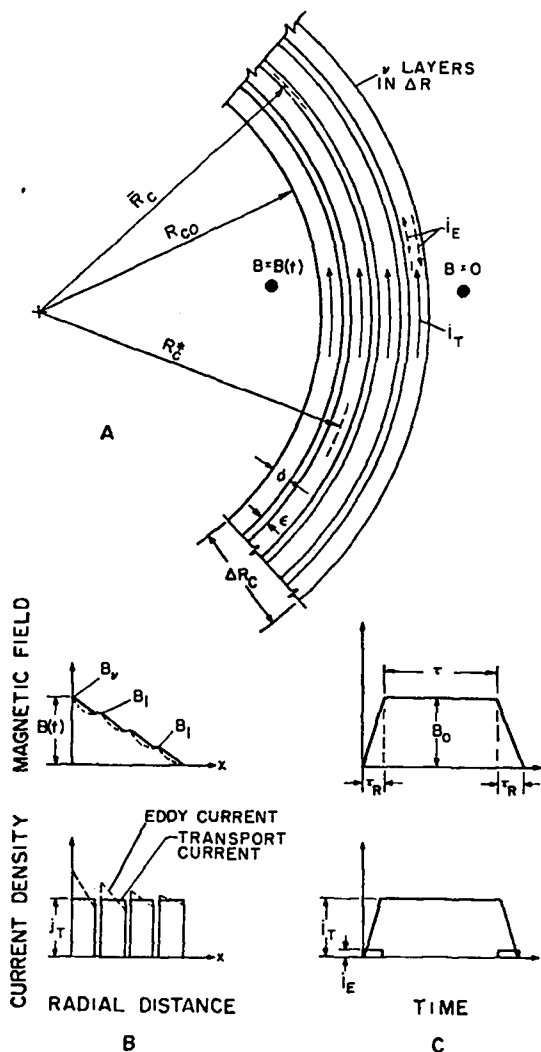   transport current, and eddy current.

C. Joule Eddy-Current Losses in the Compression Coil.

Figure 17 shows schematically the magnetic
compression pulse of the reactor, having a linearly
rising portion of duration τ_R. For such a magnetic
field the electrical skin depth (Appendix D) is
given by

$$\delta_{ER}^2 = 1/2 \times 10^8 \, \eta \tau_R . \tag{31}$$

In Appendix E the joule energy loss due to eddy cur-
rents induced in the coil during the rising and fall-
ing portions of the magnetic waveforms is shown to be

$$W_E = \frac{2\pi \overline{R}_c \, \eta \, B_o^2 \, \tau_R}{(0.4\pi)^2 \, \lambda \Delta R_c} \left(\frac{\lambda^2 \Delta R_c^2 d^2}{45.6 \, \delta_{ER}^4} \right) . \tag{32}$$

where d is the coil layer thickness. Eliminating η
between (31) and (32) yields

$$W_E = \frac{10^{-12} \, \overline{R}_c B_o^2 \, \lambda \Delta R_c d^2}{5.73 \, \delta_{ER}^2} . \quad MJ/m \tag{33}$$

The total joule loss in the compression coil during
the pulse is given by

$$W_{JC} = W_T \left[1 + \left(\frac{\tau}{\tau + 2/3 \, \tau_R} \right) \left(\frac{\lambda^2 \Delta R_c^2 d^2}{45.6 \, \delta_{ER}^4} \right) \right] . \quad MJ/m \tag{34}$$

The condition that the eddy current loss be only 2%
of the transport current loss ($W_E/W_T = 0.02$) is that

$$d^2 = \frac{45.6 \, \delta_{ER}^4}{\lambda^2 \, \Delta R_c^2} \left(\frac{\tau + 2/3 \, \tau_R}{\tau_R} \right) (0.02). \tag{35}$$

Setting $\tau_R = 10^{-2}$ sec, we find $\delta_{ER} = 0.92$ cm from
(31). For $\tau = 10^{-1}$ sec, the coil winding thickness
is given by, from (35):

$$d \leq .94 \text{ mm}.$$

This criterion is met in the coil design of Fig. 16.
For double element transmission lines and a filling
factor of $\lambda = 0.7$, the number of turns per trans-
mission line is

$$N = \frac{\lambda \Delta R_c}{(2)(32)d} = 4.5 \quad ,$$

assuming 32 feed points. The total number of turns
in the compression coil is thus 32 N, or 144 turns.
(For triple element transmission lines, N = 3 turns
for 32 feed points and the total number of turns is
96).

D. Joule Loss of Compression Field Energy in the Implosion-Heating Coil.

When the compression field B is applied it must penetrate the wall of the implosion-heating coil. It is easily shown that the resistive loss of energy W_{ES} in this penetration process is related to the energy W_{BS} which is finally stored in the implosion-heating coil by

$$W_{ES}/W_{BS} = 2\alpha/(1 + \alpha), \tag{36}$$

where α is the ratio of the L/R time of the shock-heating coil to τ_R, and we have counted losses both on the rise and fall of the B field. For a single-turn coil,

$$L/R = 2\pi b \Delta b \times 10^{-9}/P_s \eta_s \tag{37}$$

where b is the shock-coil radius and Δb is its thickness. The quantity P_s measures the ratio of length of the coil perimeter plus radial Nb transmission-line conductors to that of the coil perimeter above, assuming the coil and transmission-line conductors to have the same thickness Δb. From Fig. 16 we find $P_s = 4.4$ for b = 30 cm. For 800 °C Nb, $\eta_{Nb} \approx 6 \times 10^{-5}$ ohm-cm. For $\Delta b = 0.3$ cm we calculate L/R = 0.21 msec and $\alpha = 0.021$. The magnetic energy stored in the compression coil is given by

$$W_B = (B_o^2/8\pi)(\pi R_c^{*2}) \times 10^{-11} \text{ MJ/m} . \tag{38}$$

where R_c^* is an effective radius for magnetic energy storage (in cm),

$$R_c^* = R_{co} + \frac{\Delta R_c}{3} , \tag{39}$$

and B_o is measured in Gauss.

For R_{co} = 70 cm and ΔR_c = 40 cm, R_c^* = 83.33 cm and

$$W_B = 195 \text{ MJ/m} . \tag{40}$$

$$W_{BS} = (b/R_c^*)^2 W_B = 25 \text{ MJ/m} . \tag{41}$$

and

$$W_{ES} = 1.06 \text{ MJ/m}. \tag{42}$$

E. Eddy-Current Losses in the Blanket.

In Fig. 16 ceramic separators are shown which divide the niobium-encased lithium and carbon regions into narrow radial segments. It is easily shown that for segments of width h much less than their lengths, the eddy-current joule losses in the blanket region per unit length, W_E', normalized to the total stored magnetic energy, (38), is

$$\frac{W_E'}{W_B} = f_A \pi h^2/20 \, \delta_{ER}^2 \tag{43}$$

where f_A is the fraction of the area πR_c^{*2} which is occupied by the blanket material. For lithium at 800 °C, $\eta_{Li} \approx 1.9 \times 10^{-4}$ ohm-cm, δ_{ER} = 9.75 cm, and $f_A = 0.21$ (Fig. 15). If we limit the eddy current losses in the lithium to, say, 0.25% of W_B, then

$$W_E'(Li) = 0.5 \text{ MJ/m}$$

and $\qquad\qquad\qquad\qquad\qquad$ (44)

$$h_{Li} = 2.7 \text{ cm}.$$

For the carbon portion of the blanket we find $\eta_C \approx 2.1 \times 10^{-3}$ ohm-cm (for 1000 °C), δ_{ER} = 32 cm, and $f_A = 0.32$. For carbon eddy-current losses equal to, say, 0.1% of W_B,

$$W_E'(C) = 0.195 \text{ MJ/m}$$

and $\qquad\qquad\qquad\qquad\qquad$ (45)

$$h_C = 4.5 \text{ cm}.$$

These h values correspond to physically realistic spacings for the insulators, as illustrated in Fig. 16.

F. Summary.

All transport current losses are incurred in the compression coil, and for the RTPR design, assuming a trapezoidal current pulse, are

$$W_T = 5.24 \text{ MJ/m} .$$

The eddy-current losses have several components: W_E in the compression coil, W_{ES} in the shock coil, and $W_E'(Li)$ and $W_E'(C)$ in the blanket, and these total to

$$W_{E\text{-total}} = 1.86 \quad \text{MJ/m} \quad .$$

The eddy-current losses are adjustable in that they can be reduced by further subdivision of the electrically conducting materials in the blanket into smaller unit cells. In this design the eddy-current losses constitute 25% of the total joule losses of 7.09 MJ/m.

XIII. MECHANICAL STRESS, RADIATION, AND HEAT TRANSFER AT THE FIRST WALL

A. Time History.

In a pulsed theta-pinch reactor the mechanical, dielectric, and thermal stresses[32] in the first wall facing the plasma are cyclic with period τ_c, having approximately the time history shown schematically in Fig. 18.

During the implosion-heating phase, which lasts about 2 msec, the plasma has a density of $\sim 3 \times 10^{15}$ cm^{-3} and a temperature of ~ 5 keV (Table I). There is negligible neutron radiation and bremmstrahlung during this phase of the discharge. The sudden application of the implosion field at $t = 0$ requires of the order of 1.6 MV around the inside of the first wall, which is also the implosion-heating coil. The corresponding electrical stress in the first wall dielectric (Al_2O_3 in the RTPR) is ~ 9 kV/cm (22 V/mil) and lasts for the risetime of the current, ~ 100 nsec. The 31.8-kG implosion-heating field exerts an outward pressure of ~ 36 Atmospheres (600 psi) on the Nb coil, giving rise to a hoop stress (in the absence of radial supports):

$$S_H = \frac{pb}{\Delta b} \tag{46}$$

$$= 60,000 \text{ psi}$$

($p = 600$ psi, $b = 30$ cm, and $\Delta b = $ Nb wall thickness $= 0.3$ cm). This stress will be substantially reduced, depending on the reinforcing structure through the blanket. The L/R time of the Nb coil is ~ 200 μsec (Eq. 37), and therefore the implosion-heating circuit has crowbar capacitors (Fig. 14)
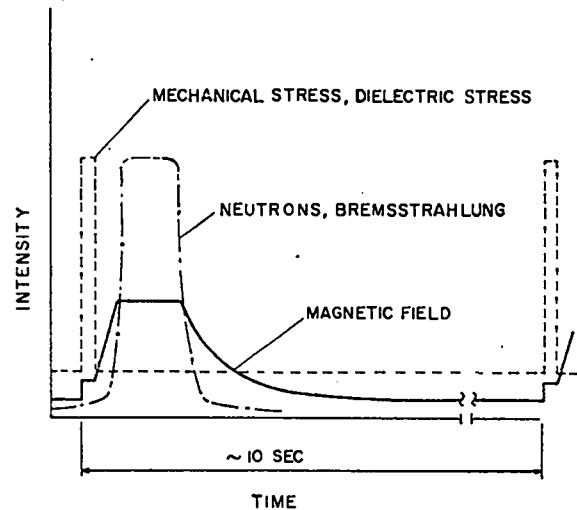

Fig. 18. Time history of the radiation and mechanical stress for the first wall of a pulsed θ pinch reactor.

to sustain the current.

During the 100 msec burn the first wall undergoes a photon flux of bremsstrahlung and cyclotron radiation, and a particle flux of 14 MeV neutrons (which penetrate the wall) and charged particles due to diffusion across the confining magnetic field B_o (which may cause first surface sputtering). A study[33] of time dependent diffusion in a theta pinch has shown that the charged particle loss to the wall during the burn is negligible (<<1%) for diffusion rates up to 100 times the classical value in the present case. The temperature rise in the Nb wall due to neutron energy deposition has been calculated to be quite small, less than 5 °C. Similarly the temperature rise due to eddy current losses in the Nb wall ($W_{ES} = 1.06$ MJ/m) is ~ 75 °C when heat conduction to the flowing Li coolant is completely neglected. When heat conduction is included in the analysis the temperature excursion in the Nb shell is limited to a few tens of °C.

B. Bremsstrahlung Absorption.

In the RTPR a major source of first wall heat is bremsstrahlung absorption.

With the inclusion of burnup effects, the incident bremsstrahlung energy flux on the first wall is given by

$$\phi_{BR} = \left(\frac{W_{BR}}{W_{BR_o}}\right) \frac{W_{BR_o}}{2\pi b} \quad MJ/m^2 \tag{47}$$

where the quantity (W_{BR}/W_{BR_o}) is plotted in Fig. 11 and W_{BR_o} is given by Eq. (22). We find

$$\phi_{BR} = 0.57 \quad MJ/m^2 .$$

The bremsstrahlung radiation is peaked at a wavelength[34] which is a function of kT_e :

$$\lambda_{BR} = \frac{6.200}{kT_e (keV)} \quad \overset{\circ}{A} . \qquad (48)$$

From the T_e curve in Fig. 10, the electron temperature is seen to vary from a starting value of 15 keV to 38 keV (Table III) during the burn. Assuming an average value of 25 keV, the wavelength $\lambda_{BR} = 0.25 \overset{\circ}{A}$ is found to lie in the hard x-ray region of the spectrum.

A computer study has been made of the absorption of the bremsstrahlung spectrum from plasmas of various temperatures on a composite Al_2O_3 – Nb first wall. Figure 19 shows the result, where we plot the percent of the total incident energy which is absorbed vs. the thickness of the Al_2O_3 insulator. Corresponding to 25 keV and 1-mm thickness of Al_2O_3, approximately 60% of ϕ_{BR}, or 0.34 MJ/m^2, is absorbed in the first wall insulator. The remaining 40% is transmitted to the Nb interface where it is absorbed in a very thin layer (~ 0.01 mm), owing to the high atomic mass number. The Nb wall has a thickness $\Delta b \approx 3$ mm, and its outer surface is maintained at an assumed constant temperature of 800 °C by the liquid Li flow.

The radiated cyclotron energy (peak wavelength ~ 1 mm) lies in the far infrared region of the spectrum where it is easily reflected by the walls. The high plasma beta and self-absorption effects limit cyclotron radiation to less than 1% of the bremsstrahlung radiated energy.[33]

C.   Temperature Rise.

A detailed radiation-absorption and heat-transfer study has been done numerically for the composite first wall described above, and the results are shown in Fig. 20. The incident bremsstrahlung has been computed as a function of time from the burnup code of Sec. VIII. The absorption as a function of distance and time in the
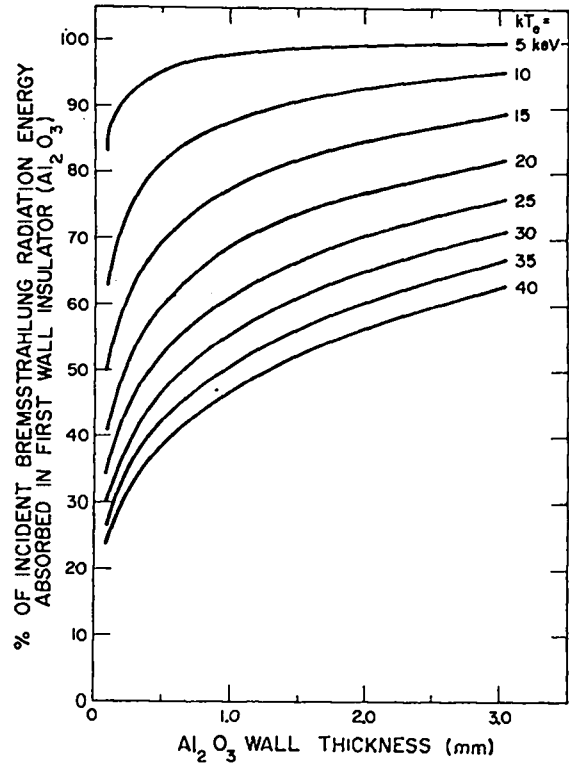
Fig. 19.   The percent of incident bremsstrahlung radiation energy which is absorbed in the first wall insulator (Al_2O_3) plotted against the wall thickness, for a number of different values of the electron temperature of the plasma which emits the radiation.

Al_2O_3 is then derived from the curves of Fig. 19, and the heat conduction equation is solved for the resultant temperature distribution in the wall as a function of time. The burn is assumed to stop at 100 msec, and the plasma to cool down so as not to produce any further significant bremsstrahlung radiation thereafter. The $T(r)$ profiles in Fig. 20 are plotted for six successive times, starting at 10 msec after the beginning of the burn. Each curve is also identified by the dimensionless quantity $(\Delta r + \Delta b)/\delta_T(Nb)$, where $\Delta r + \Delta b$ is the total wall thickness (4 mm in this case), and δ_T is the thermal skin depth for niobium,

$$\delta_T = \sqrt{\frac{2}{\pi} \frac{K_v}{C_v} t} \qquad (49)$$

$$= 0.41 \quad \sqrt{t} \quad cm$$

Fig. 20. Temperature profiles in the composite Al$_2$O$_3$-Nb first wall, resulting from bremsstrahlung energy absorption (see Fig. 19), plotted for various times during the burn and subsequent cooling.

where t is the time in sec. The maximum temperature excursion in the wall, shown by curve c, is ~ 100°C and occurs at 100 msec on the inside surface. After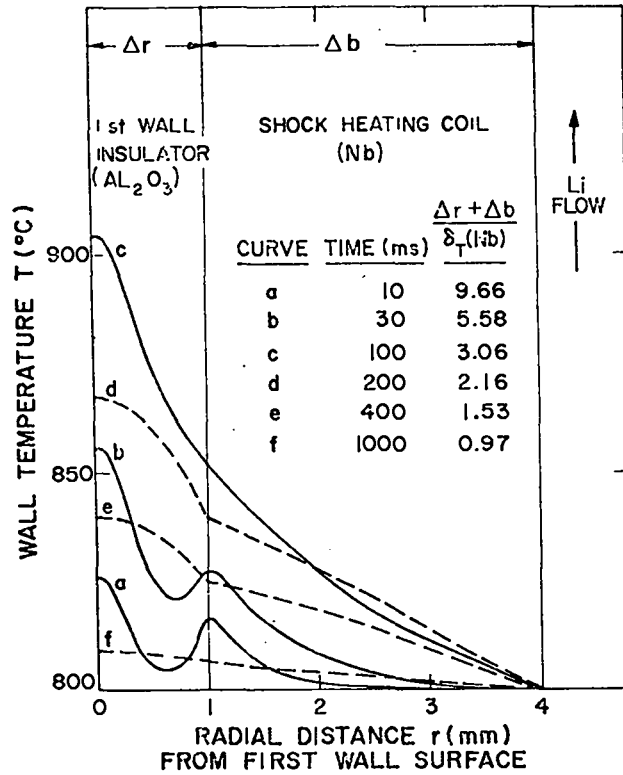 1 sec (curve f) the temperature profile is nearly flat once more, and the wall is ready for another cycle. The quantity $(\Delta r + \Delta b)/\delta_T$ (Nb) is approximately unity at 1 sec, and the thermal skin depth δ_T (Nb) is thus a good measure of the distance over which heat can be removed from the first wall by the flowing Li coolant.

XIV. ENERGY BALANCE, CIRCULATING POWER FRACTION, AND PLANT EFFICIENCY

Considering the overall energy balance of the reactor we take account of the core and compression coil joule losses and make an estimate of the expenditure of energy W_A used in driving the electrical generating plant and auxiliaries such as coolant pumps. There is in addition an energy loss W_{SC} in the cryogenic circuit which will depend on the choice of superconducting or cryogenic materials used.

In describing the energy balance, we use the quantity M to indicate the excess of electrical energy over losses.[35] Thus

$$\eta_T \left[W_n + W_{BR} + (W_p)_f + (N_\alpha E_\alpha)_f + W_{ES} + W_E^-(Li) + W_E^-(C) \right]$$

$$= M \left[(W_p)_i + (W_L - \Delta W) + W_{SC} \right] \qquad (50)$$

$$\eta_T \left(W_0 \right) = M W_i \qquad (51)$$

where the bracket on the left side of Eq. (50) represents energy available as high grade heat (~800°C) and the bracket on the right represents energy losses which must be supplied during each burning pulse. Table IV defines the various quantities appearing in Eqs. (50) and (51), and their calculated magnitudes are given for a burning time of τ = 100 msec. The final plasma energy, for example, is given by

$$\left(W_p \right)_f = \frac{3}{2} \left[n_{ef} \ kT_{ef} + n_f \ kT_{if} \right] \pi a_f^2 \quad , \qquad (52)$$

where the various quantities appearing in (52) can be found in Table III. Note that the energy multiplication factor Q (the ratio of total reactor energy W_0 to the total plasma preparation energy W_i), is given by

$$Q = \frac{W_0}{W_i} = \frac{M}{\eta_T} \quad . \qquad (53)$$

The plant circulating-energy fraction is

$$\epsilon = \frac{W_C}{W_g} = \frac{1}{M} \left(1 + \frac{W_A}{W_i} \right) \quad . \qquad (54)$$

The quantity W_A is the energy per pulse associated with operating the electrical power plant and auxiliaries such as coolant pumping. We assume $\frac{W_A}{W_g} \approx 3\%$. In addition, the losses W_{SC} in the superconducting energy storage circuit of the reactor, a quantity presently unknown, must be taken into account. If we limit W_{SC} to, say, 0.5% of W_{BO} (the peak energy stored in the cryogenic system), then

$$W_{SC} = 1.57 \quad MJ/m$$

21

TABLE IV

ENERGY VALUES IN THE REFERENCE THETA PINCH REACTOR

Symbol	Definition	Value	
$(W_p)_i$	Initial Plasma Energy $= 3n_o kT_o (\pi a_o^2)$	3.41	MJ/m
W_{ES}	Joule Eddy Current Losses in Shock Heating Coil	1.06	MJ/m
$W_E^-(Li)$	Joule Eddy Current Losses in Li Blanket	.50	MJ/m
$W_E^-(C)$	Joule Eddy Current Losses in C Blanket	.19	MJ/m
W_E	Joule Eddy Current Losses in Compression Coil	.10	MJ/m
W_T	Joule Transport Current Losses in Compression Coil	5.24	MJ/m
W_L	Resistive Energy Losses (total) $= W_{ES} + W_E^-(Li) + W_E^-(C) + W_E + W_T$	7.09	MJ/m
W_{SC}	Energy Losses in Cryogenic Magnetic Energy Storage System	1.57	MJ/m
ΔW	Direct Conversion Energy (High-β Plasma Expansion)	6.14	MJ/m
W_i	Total Plasma Preparation Energy $= (W_p)_i + W_L + W_{SC} - \Delta W$	5.93	MJ/m
W_{BR}	Bremsstrahlung Energy Loss	1.08	MJ/m
W_n	Thermonuclear Neutron Energy ($Q_n = 18.9$ MeV)	88.40	MJ/m
$(W_p)_f$	Final Plasma Energy	6.88	MJ/m
$(N_\alpha E_\alpha)_f$	Final Alpha Particle Energy	5.70	MJ/m
W_O	Total Reactor Energy $= W_{BR} + W_n + W_{ES} + W_E^-(Li) + W_E^-(C) + (W_p)_f + (N_\alpha E_\alpha)_f$	103.81	MJ/m
W_g	Gross Electrical Energy $= \eta_T W_O$	60.21	MJ/m
W_A	Thermal Conversion Losses $= 3\% W_g$	1.80	MJ/m
W_C	Circulating Energy $= W_i + W_A$	7.73	MJ/m
W_e	Net Electrical Energy ($= W_g - W_C$)	52.48	MJ/m
W_{BO}	Peak Magnetic Energy in Cryogenic System	315.	MJ/m
η_T	Thermal Conversion Efficiency	58%	
η_M	Direct Conversion Efficiency	100%	
η_P	Overall Plant Efficiency	50.1%	
Q	Energy Multiplication Factor $= W_O/W_i$	17.5	
ϵ	Fractional Circulating Power $= W_C/W_g$	12.8%	
M	Excess of Electrical Energy Over Losses	10.2	

TABLE IV

(continued)

τ	Burning Time	100 msec
τ_c	Cycle Time	10 sec
ξ^{-1}	Duty Factor $(= \tau/\tau_c)$	0.01
P_T	Reactor Thermal Power $= W_0 L/\tau_c$	3.6 GW_{th}
P_e	Reactor Net Electrical Power $= \eta_p P_T$	1.8 GW_e
L	Reactor Length	350 m

and

$$\epsilon = 12.8\%$$
$$M = 10.2$$
$$Q = 17.5 \quad .$$

The Carnot efficiency of an ideal heat engine working between an upper temperature of 800 °C (1100 °K) and a lower temperature of 300 °K is (1100 - 300)/1100 = 0.73. By using a potassium topping cycle, as shown in Fig. 21, the actual thermal efficiency of an operating plant may be greater than 60%. We will assume $\eta_T = 0.58$ in the present study. The overall plant efficiency

$$\eta_p = \eta_T (1 - \epsilon) \tag{55}$$

is then 50.1%.

In this discussion we have followed the parameter definitions suggested by Persiani, et al.[36] Figure 22 is an energy flow diagram for the pulsed θ-pinch reactor which also follows the usage given by these authors.

An inspection of Table IV shows that the dominant term in the energy balance equation is W_n, as indeed it must be if losses are to be small compared to the thermonuclear power. The quantities W_n, W_{BR}, $(W_p)_f$, $(n_\alpha E_\alpha)_f$ and ΔW are computed by means of the burnup code described in Sec. VIII. We note that the energy produced by direct conversion ($\Delta W = 6.14$ MJ/m) as the high-β plasma expands against the confining magnetic field during the burn nearly equals the total joule losses ($W_L = 7.09$ MJ/m) in the reactor core, thus substantially
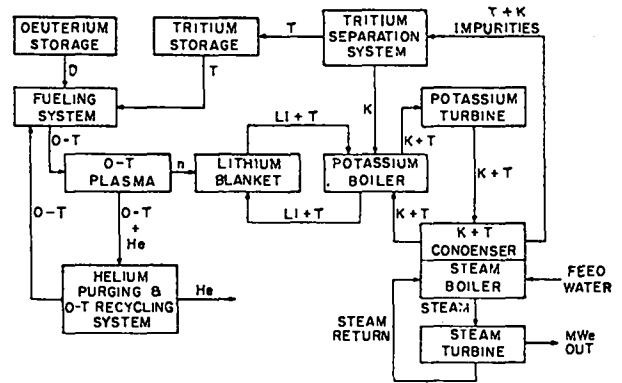
Fig. 21. Block diagram of possible tritium separation and energy-removal systems.

reducing the circulating power requirements of the reactor. The circulating power fraction (12.8% in the present example) can be reduced below 10% quite readily by increasing the burn time (to 125 msec, for example), or by increasing the magnetic field (to 165 kG, for example) [see Eq. 12]. In fact it seems clear that the flexibility of the pulsed system, through its adjustable duty cycle, permits the perturbation of the present reference reactor into a system with an arbitrarily small circulating power fraction.

XV. INTEGRATED WALL LOADING, DUTY FACTOR, AND PLANT ELECTRICAL OUTPUT

A. Wall Loading

The duty factor of the reactor ξ^{-1} is related to the burn time ($\tau = 0.10$ sec) by

$$\xi^{-1} = \tau/\tau_c \quad . \tag{56}$$

23

The cycle time τ_c is determined by the requirement that the average first wall nuclear throughput,

$$P_W = \frac{W_n}{2\pi b \; \tau_c} \quad \frac{14.06 \text{ MeV}}{Q_n} \qquad (57)$$

where $Q_n = 18.9$ MeV, be limited to 3.5 MW/m^2 (350 W/cm^2). For $W_n = 88.4$ MJ/m (Table IV), Eq. (57) gives

$$\tau_c = 10 \text{ sec.}$$

The corresponding average primary neutron fluence on the first wall (i.e. neglecting backscatter) is 1.4×10^{15} neutrons/cm^2/pulse. The time averaged primary neutron current is 1.4×10^{14}/cm^2/sec) and during the burn the instantaneous current is 1.4×10^{16}/cm^2/sec. The primary neutron current accounts for approximately 1/4 of the total neutron flux through the first wall. The primary neutron current integrated over one year of continuous operation of the reactor is 4.4×10^{21} neutrons/cm^2/yr through the first wall.

B. Plant Thermal and Electrical Power

The thermal power of the reactor is

$$P_T = \frac{W_0 L}{\tau_c} \quad \text{MW} \quad , \qquad (58)$$

where $W_0 = 103.8$ MJ/m (Table IV), and L is the length of the reactor in meters. For a reactor length of 350 m (toroidal major radius = 56 m), we have

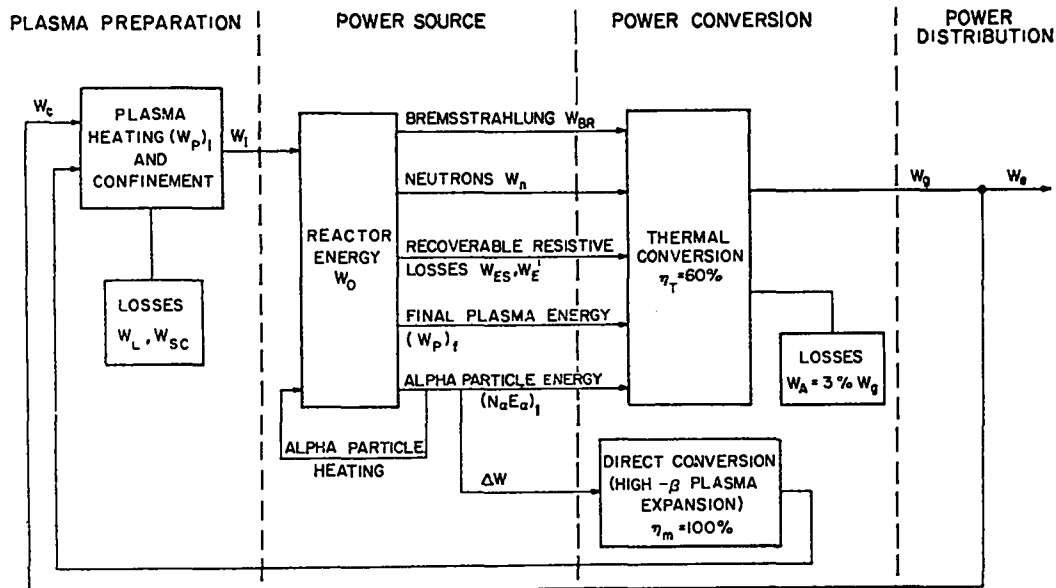$$P_T = 3.63 \quad \text{GW.}$$

Fig. 22. Energy Flow Diagram for Reference Theta Pinch Reactor

The net electrical power output (power on the line) is

$$P_e = \eta_p P_T \qquad (59)$$

where $\eta_p = 50.1\%$ is the overall plant efficiency. Hence

$$P_e = 1.82 \quad GW \ .$$

The power output per unit length is $1820/L = 5.2$ MW/m, and the energy output "on the line" per unit length of reactor is

$$W_e = P_e \tau_c / L \qquad (60)$$

$$= 52 \quad MJ/m/pulse \ .$$

A figure of merit which is sometimes applied to thermonuclear reactors is the ratio of the magnetic energy stored in the cryogenic system to the electrical power output. Thus

$$\frac{W_{Bo}}{(P_e/L)} = \frac{315}{5.2} = 61 \quad J/W. \qquad (61)$$

C. Direct Conversion

The direct conversion energy ΔW expressed as a fraction of the output energy is

$$\frac{\Delta W}{W_e} = \frac{6.14}{52} = 12\% \ . \qquad (62)$$

It was found in Section VIII that the direct conversion energy expressed as a fraction of the neutron energy deposited in the blanket was 7%, i.e.

$$\frac{\Delta W}{W_n} = 0.07 \ .$$

The difference between 12% and 7% is not unlike the thermal efficiency of the reactor power plant, i.e., 50%.

XVI. CONCLUSIONS

As opposed to a steady-state system, a pulsed thermonuclear reactor is considerably different both in its plasma physics characteristics and in the approach to basic design problems. The pulsed device we have outlined operates at a high beta value and at higher plasma densities than steady-state reactors, but since the pulsed system is "on" for only a few percent of time an acceptable wall loading can be realized with a much smaller vacuum chamber radius than in steady-state systems such as Tokamaks.

There are other significant advantages in using a pulsed high-beta plasma as the reactor energy source. They include the fact that there is no flow of liquid metal across magnetic field lines during 98% of the coolant cycle. The pulsed containment field lies outside the superconducting coil and thus the value of the superconducting magnetic field is independent of that of the compressional field. Fueling and flushing of the plasma between burning pulses can probably be accomplished without divertors by continuously flowing D-T gas through the discharge chamber. During this recycling process heat transfer from the plasma to the first wall is expected to depend primarily on atom thermal transport and visible and uv radiation in the region of neutral gas surrounding the core. Direct energy conversion by the expansion of the high-beta plasma against the confining magnetic field during burning (about 7% of the thermonuclear energy and ~12% of the electrical energy) furnishes the joule losses in the room temperature compression coil. The calculations of Section XV indicate that no net electrical input to the magnetic compression system may be necessary.

The reactor parameters presented here are not unique; however, they are self consistent and provide for a reasonable energy balance and circulating power fraction. Iterations are planned in the future to improve these results, by varying the reactor parameters B_o, τ, kT_o, etc. in the calculations. Final parameters will be obtained on the basis of scientific information gained in the Scyllac experiment[37,38] and later experiments[39] which demonstrate the staged θ-pinch concept, as well, of course, as future technological developments.

I. A MODEL OF IMPLOSION HEATING

In the model[6,8] taken here (see Fig. 2), a sheath separating a magnetic field B_s and the plasma advances radially inward at a speed u_s, projecting ions ahead of it at a speed $2u_s$. The ambient plasma filling density inside this "magnetic piston" is n_A, and the plasma ahead of the piston is assumed to be relatively cold (~ 1 ev). Only ions are assumed to gain energy, and the electrons remain cold but fully ionized. (In practice there is some joule heating of the electrons in the sheath; however, this heating is much less than that of the ions.) Plasma-simulation studies[9] show that the actual process whereby the ions are given a spread of energies from an ideal sheath can be one of repeatedly bouncing off the sheath wall as they pass through the center of the discharge tube, leading to piston oscillations which finally (on a scale of 0.1 μsec) settle down to some sheath radius bx_{SH} at the end of the shock phase.

Simple dynamical considerations show that the first ions projected from the sheath will hit it again after passing through the axis of the discharge when the sheath has advanced to $x = 1/3$. As an average approximation to the actual train of events we assume that all of the ions inside the sheath at this instant thermalize to a temperature T_{SH} and then push the sheath back to x_{SH}, doing an amount of work $(B_s^2/8\pi)\pi b^2[x_{SH}^2 -(1/3)^2]$ against the constant field B_s. Hence

$$\pi b^2 n_A[1 - (1/3)^2] [1/2\ m_i(2u_s)^2] = 3/2\ \pi b^2 n_A kT_{SH}$$

$$+ 1/8\ b^2 B_s^2[x_{SH}^2 - (1/3)^2], \tag{A-1}$$

where m_i is the ion mass.

The momentum of the projected ions is related to B_s by

$$B_s^2/8\pi = 2m_i n_A u_s^2. \tag{A-2}$$

After the piston-heated plasma becomes quiescent, pressure balance requires

$$(n_A/x_{SH}^2)kT_{SH} = B_s^2/8\pi\ . \tag{A-3}$$

Substituting (A-3) and (A-2) into (A-1) we find

$$x_{SH} = (2/5)^{1/2} = 0.632\ . \tag{A-4}$$

Note that $u_s = (kT_{SH}/2m_i)^{1/2}/x_{SH} = 2.20 \times 10^7$ $[kT_{SH}(keV)]^{1/2}$. The initial back emf around the inside of the discharge tube is given by

$$V_s = 2\pi \times 10^{-8}\ bu_s B_s \quad \text{(Volts)}. \tag{A-5}$$

Substituting Eqs. (A-2) and (A-3),

$$V_s = 10^{-8} \left(\frac{\pi}{4m_i n_A}\right)^{1/2} bB_s^2$$

$$= 4 \times 10^{-8} \left(\frac{\pi^3 n_A}{m_i}\right) \frac{bkT_{SH}}{x_{SH}^2}\ . \tag{A-6}$$

In more convenient units (for $m_i = 4.15 \times 10^{-24}$ g, an "average" D-T ion),

$$V_s(kV) = 0.517 \times 10^{-6}\ b\ B_s^2/p_A^{1/2}$$

$$= 3.68\ p_A^{1/2} bkT_{SH}(keV), \quad (x_{SH} = 0.632) \tag{A-7}$$

where p_A is the ambient filling pressure in mTorr, b is in cm and B_s is in gauss.

II. EQUILIBRATION OF IONS AND ELECTRONS

After the implosion, but before the slow adiabatic compression has progressed very far, the electrons and ions will come to the same temperature T_E by means of collisions. We assume this process to begin at $x = x_{SH}$, $T_i = T_{SH}$, $T_e = 0$ and to end at $x = x_E$, $T_i = T_e = T_E$, while the magnetic field maintains the constant value B_s. Thus

$$T_E = \frac{1}{2} T_{SH} \tag{A-8}$$

$$x_E = x_{SH} \tag{A-9}$$

$$a_E = a_{SH} \tag{A-10}$$

and we write (A-3) as

$$2n_A k T_E = x_{SH}^2 (B_s^2/8\pi). \qquad \text{(A-11)}$$

III. ADIABATIC COMPRESSION

During compression the plasma behaves as a gas with specific heat ratio $\gamma = 5/3$, such that, from Sec. III, Eqs. (1) and (2), $(kT) a^{2(\gamma-1)} = $ constant. If subscript "o" refers to the plasma state at the end of the compression, then

$$T_o = T_E \left(\frac{x_{SH}}{x_o}\right)^{2(\gamma - 1)} \qquad \text{(A-12)}$$

$$n_o = n_A/x_o^2 . \qquad \text{(A-13)}$$

Pressure balance, $2nkT = B^2/8\pi$, then requires

$$B_o/B_s = (x_{SH}/x_o)^\gamma = (T_o/T_E)^{\left[\frac{\gamma}{2(\gamma - 1)}\right]}, \qquad \text{(A-14)}$$

where the final compression field is given by

$$B_o(kG) = 2.386 \frac{[p_A k T_o (keV)]^{1/2}}{x_o} . \qquad \text{(A-15)}$$

Substituting (A-6) and (A-11) into (A-12), we obtain (for $\gamma = 5/3$)

$$kT_o = \frac{10^8}{8\pi^{3/2}} \frac{x_{SH}^{2\gamma}}{x_o^{2(\gamma - 1)}} \frac{m_i^{1/2}}{n_A^{1/2}} \frac{V_s}{b} \qquad \text{(A-16)}$$

$$kT_o(keV) = 0.0737 \frac{V_s(kV)}{b p_A^{1/2} x_o^{4/3}} . \qquad \text{(A-17)}$$

IV. SHOCK FIELDS PROGRAMMED FOR FREE EXPANSION OF THE IONS

In order to obtain lower compression (larger x_{SH}) for a given B_s and V_s, a magnetic field having the time history shown in Fig. A-1 may be used.[10] An initial piston field of magnitude $2^{-1/2} B_s$ is suddenly removed at time t_1 when the sheath has arrived at $x = 1/3$. A larger field is reapplied at $3/2\ t_1$, when all ions have advanced to approximately the opposite wall, and reflects them all at velocity $2u_s$. In contrast to expression (A-2), we now have

$$B_s^2/8\pi = 4 n_A m_1 u_s^2 . \qquad \text{(A-18)}$$

We denote the temperature of the thermalized ions after the free expansion and reflection by T_{SH}' and the fractional tube radius by x_{SH}'. Thus

$$(x_{SH}')^2 B_s^2/8\pi = n_A k T_{SH}' . \qquad \text{(A-19)}$$

Note that $u_s = (kT_{SH}'/4m_1)^{1/2}/x_{SH}' = 1.29 \times 10^7 [kT_{SH}'(keV)]^{1/2}$. Corresponding to (A-1) we now have

$$\pi b^2 n_A [1 - (1/3)^2][1/2\ m_1 (2u_s)^2] \qquad \text{(A-20)}$$

$$= 3/2\ \pi b^2 n_A k T_{SH}' - 1/8\ b^2 B_s^2 (1 - x_{SH}'^2),$$

where the last term represents work done on the plasma after the velocity-reversing reflection. Solving (A-20), (A-19) and (A-18) yields

$$x_{SH}' = (26/45)^{1/2} = 0.76. \qquad \text{(A-21)}$$

Since the ions are accelerated by $2^{-1/2} B_s$, we have

$$V_s' = 2^{1/2} \pi \times 10^{-8} b u_s B_s$$
$$= 10^{-8} \left(\frac{\pi}{16 m_1 n_A}\right)^{1/2} b B_s^2 ; \qquad \text{(A-22)}$$

$$V_s'(kV) = 0.259 \times 10^{-6} b B_s^2 / p_A^{1/2}$$
$$\qquad \text{(A-23)}$$
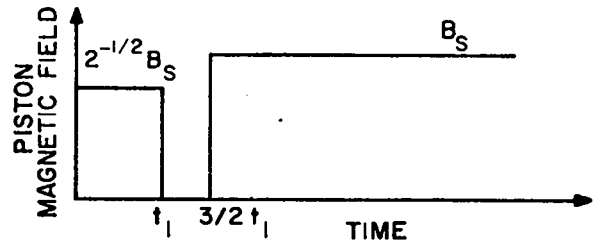$$= 1.275\ p_A^{1/2} b k T_{SH}'(keV). \qquad (x_{SH}' = 0.76)$$

Fig. A-1. Time history of magnetic field for free expansion of the ions following the initial sheath implosion.

After adiabatic compression, the plasma temperature is thus

$$kT'_o = \frac{10^8}{4\pi^{3/2}} \; \frac{(x'_{SH})^{2\gamma}}{x_o^{2(\gamma-1)}} \; \frac{m_i^{1/2}}{n_A^{1/2}} \; \frac{V'_s}{b}; \quad \text{(A-24)}$$

$$kT'_o \text{ (keV)} = 0.272 \frac{V'_s \text{(kV)}}{b p_A^{1/2} x_o^{4/3}}$$

$$\text{(A-25)}$$

for $x'_{SH} = 0.76$.

APPENDIX B

MAGNETIC ENERGY TRANSFER AND STORAGE

From the circuit of Fig. 6 (a), the flux linkage in each circuit is constant:

$$L_1 i_1 + M_{21} i_2 + M_{31} i_3 = \text{const}$$

$$L_2 i_2 + M_{21} i_1 = \text{const}$$

$$(1 + \ell)L_3 i_3 + M_{31} i_1 + M_{PS} i_4 = \text{const}$$

$$(1 + m) L_4 i_4 + M_{PS} i_3 = \text{const}.$$

In normalized form, with $x_j = \sqrt{L_j}\, i_j$ and $\beta = k_T \sqrt{\ell m}$,

$$x_1 + k_{21} x_2 + k_{31} x_3 = y_1$$

$$x_2 + k_{21} x_1 = y_2$$

$$\quad \text{(B-1)}$$

$$(1 + \ell) x_3 + k_{31} x_1 + \beta x_4 = y_3$$

$$\beta x_3 + (1 + m) x_4 = y_4 .$$

We also define $k_{ij}^2 L_i L_j = M_{ij}^2$.

Now if the system is energized with coils 1 and 2 uncoupled the flux linkage $y_2 = 0$. Solutions to Eq. (B-1) are then

$$K x_1 = y_1$$

$$x_2 = - k_{21} x_1 \quad \text{(B-2)}$$

$$x_3 = - \alpha k_{31} x_1$$

$$x_4 = b(k_m + k_{31}) x_1$$

where

$$b = \frac{\beta}{1 + \ell + m + \ell m(1 - k_T^2)}$$

$$\alpha = \frac{1 + m}{1 + m + \ell + \ell m(1 - k_T^2)} = \frac{1 + b}{1 + \ell} < 1 \quad \text{(B-3)}$$

$$K = 1 - k_{21}^2 - \alpha k_{31} x_1 \quad \text{(B-4)}$$

$$k_{21} = k_o \cos \theta \quad \text{(B-5)}$$

$$k_{31} = k_m \sin \theta . \quad \text{(B-6)}$$

The θ variation in (B-5) and (B-6) is a property of the spherical coils in quadrature.

To find the condition under which the energy is independent of angle we calculate the total stored energy in the system:

$$W = \frac{1}{2} [x_1^2 + x_2^2 + x_3^2(1 + \ell) + x_4^2(1 + m)] + k_{21} x_1 x_2$$

$$+ k_{31} x_1 x_3 + \beta\, x_3 x_4 = \frac{1}{2} (K + \alpha b\, k_m^2) x_1^2 .$$

The above equation is independent of angle if $K =$ constant, since $K =$ constant also makes x_1 constant. A constant K is achieved if the coil radii are related by:

$$\left(\frac{R_2}{R_3}\right)^3 = \frac{k_o^2}{k_m^2} = \alpha < 1 . \quad \text{(B-7)}$$

Then,

$$W = \frac{1}{2} (1 - k_o^2 + bk_o^2) \, x_1^2 \, , \tag{B-8}$$

$$\frac{W_4}{W} = \frac{4k_T^2 \, k_m^2 \, \ell_m}{\left(\frac{\beta}{b}\right)^2 - k_m^2 \, (1 + m) \left[\frac{\beta}{b} - k_T^2 \, \ell_m\right]} \, . \tag{B-9}$$

This ratio is maximized when

$$\ell_1 = \frac{1 + m}{1 + m(1 - k_T^2)} \left[1 - k_m^2 + \frac{mk_m^2 k_T^2}{1 + m}\right]^{1/2} \, . \tag{B-10}$$

The transferred energy is further maximized by making $m = m_1$; that is,

$$\left.\frac{W_4}{W}\right]_{\ell = \ell_1} = g(m)$$

and $g(m_1)$ is a maximum. For reasonable choices of coupling coefficients, i.e. $k_T^2 = 0.98$ and $k_m^2 = 0.9$, we find $\ell_1 = 1.811$, $m_1 = 1.38$, and $g(m_1) = 0.6232$.

These values were used in the design discussed in Sec. VII.

APPENDIX C

CIRCUIT ARRANGEMENT FOR DRIVING COMPRESSION CURRENT THROUGH IMPLOSION-HEATING TRANSMISSION LINES

A schematic diagram for accomplishing the circuit connections is shown in Fig. C-1, where for simplicity we show an implosion-heating coil fed by a single Blumlein (3-conductor) transmission line of one turn. Here the left-hand compression coil carries current clockwise from a secondary-coil feed over its length (not shown, but of the order of 1 m). This current then flows axially to the right-hand compression coil and emerges clockwise to the other secondary-coil feed. In order to keep the voltage in the implosion-heating coil from being induced and multiplied in the multiple turns of compression coil two alternatives are possible: (a) The two resistors shown by dashed lines may be used to provide short circuits to the fast changing return flux of the implosion-heating coil, thus allowing no net flux to thread the compression coil. The resistors (e.g., thin stainless-steel straps) would be permeable to the slowly rising compression field as it flows through them with negligible energy loss. (b) The fast return flux can be allowed to thread all of the coiled-up turns. Adjacent compression coils are shorted together at their inputs by the small capacitor shown by means of the dashed lines. The induced voltage is absorbed in the multiple coiled-up turns.

At the outer ends of each of the transmission lines are shown two spark gaps. The inner one initiates the transmission line voltage wave from its charged center conductor. The outer spark gap is used to switch on its series capacitor to sustain the implosion-heating field until the compression field "overtakes it" in the adiabatic compression process (cf. Fig. 5). The chokes allow passage of the slowly changing compression current to the three transmission-line conductors in parallel while absorbing the implosion-heating voltages.
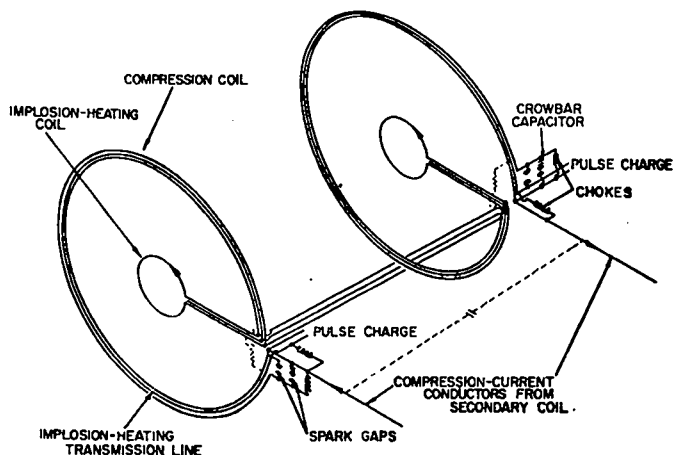

Fig. C-1. Schematic diagram showing dual use of the coiled-up implosion-heating transmission lines as compression coils.

APPENDIX D

SKIN DEPTH FOR A LINEARLY RISING MAGNETIC FIELD

Maxwell's equations with Ohm's law can be stated:

$$\nabla \times \vec{E} = 10^{-8} \frac{\partial \vec{B}}{\partial t} \tag{D-1}$$

$$\nabla \times \vec{B} = \frac{0.4\pi}{\eta} \vec{E} \;, \tag{D-2}$$

where η is the resistivity in ohm-cm, B is in gauss and E is in volt/cm. Thus

$$\frac{\partial \vec{B}}{\partial t} = \frac{10^9 \eta}{4\pi} \nabla^2 \vec{B}. \tag{D-3}$$

The corresponding (heat flow) expression of Carslaw and Jaeger (Ref. 31, p. 32)

$$\frac{\partial B}{\partial t} = K \frac{\partial^2 B}{\partial x^2} \;, \qquad K = \frac{10^8 \eta}{0.4\pi} \;. \tag{D-4}$$

Taking

$$B\big|_{x=o} = B_o\, t/\tau_R \;, \quad 0 \leqslant t \leqslant \tau_R$$

we find (Ref. 31, p. 63, case (ii))

$$B(x,t) = 4\, B_o \frac{t}{\tau_R} \; i^2 \mathrm{erfc}\left(\frac{x}{2\sqrt{Kt}}\right). \tag{D-5}$$

At $t = \tau_R$, the fractional value of B is

$$\frac{B(x,\tau_R)}{B_o} = 4\, i^2 \mathrm{erfc}(y) \tag{D-6}$$

$$y = \frac{x}{2\sqrt{K\tau_R}} \tag{D-7}$$

In particular, we are interested in the e^{-1} value of $B(x,\tau_R)$. From Carslaw and Yaeger, p. 485, this occurs at $y = 0.40$. Thus, setting $x = \delta_{ER}$,

$$\frac{\delta_{ER}}{2\sqrt{K\tau_R}} = 0.40 \tag{D-8}$$

and

$$\delta_{ER}^2 = 0.51 \times 10^8\, \eta\, \tau_R \tag{D-9}$$

$$\simeq \frac{1}{2} \times 10^8\, \eta\, \tau_R \;, \tag{D-10}$$

where δ_{ER} is identified as the electrical skin depth appropriate to the linearly rising (or falling) portion of the magnetic field waveform.

APPENDIX E

JOULE HEATING IN A MULTITURN COIL DURING A TRAPEZOIDAL CURRENT PULSE

We consider the situation illustrated in Fig. 17A where a ν-layered coil has applied to it a trapezoidal pulse of magnetic field and transport current with risetime τ_R and duration τ. During the risetime there is a component j_E of eddy current density which is small compared to the transport current density j_T. The total current density is

$$j = j_T + j_E \;. \qquad (j_E \ll j_T) \tag{E-1}$$

The coordinate $x = 0$ is taken at the left edge of the ith current layer. We treat the problem of eddy-current loss during the linear rise of B and j_T.

From Ampere's law, B and j in the conductor are related by

$$\frac{\partial B}{\partial x} = 0.4\, \pi j. \tag{E-2}$$

Substituting (E-1) and integrating over x in the ith conductor (cf. Fig. 17A),

$$B = B_i + 0.4\pi \int_0^x \left(j_T + j_E\right) dx. \qquad (E-3)$$

Ohm's law and Faraday's law of induction give

$$\frac{\partial j}{\partial x} = \frac{-10^{-8}}{\eta} \frac{\partial B}{\partial t}, \qquad (E-4)$$

where j is given by (E-1); B is given by (E-3); and η is the coil resistivity in ohm-cm. Substituting and noting that $\partial j_E/\partial t = \partial j_T/\partial x = 0$, we have

$$\frac{\partial j_E}{\partial x} = \frac{-10^{-8}}{\eta} \left[\frac{\partial B_i}{\partial t} + 0.4\pi \frac{\partial j_T}{\partial t} x\right]$$

$$= \frac{-10^{-8}}{\eta \tau_R} \left[B_i + 0.4\pi j_T x\right].$$

Integrating,

$$j_E = \frac{10^{-8}}{\eta \tau_R} \left(B_{io} x + 0.4\pi j_T \frac{x^2}{2} + C\right),$$

where B_{io} is the field strength at time τ_R at the ith conductor, corresponding to $B_o = 150$ kG for the field inside ν conductors. C is a constant such that $\int_0^d j_E dx = 0$, in order that j_E have no transport component. Thus

$$j_E = \frac{-10^{-8}}{\eta \tau_R} \left[B_{io} \left(x - \frac{d}{2}\right) + 0.4\pi j_T \left(\frac{x^2}{2} - \frac{d^2}{6}\right)\right]. \qquad (E-5)$$

Substituting (E-5) into (E-1), and noting that

$$B_{io} = \frac{i}{\nu} B_o = 0.4\pi j_T \, id$$

and

$$\delta_{ER}^2 = \frac{1}{2} \times 10^8 \, \eta \tau_R$$

(Appendix D), we obtain

$$j_i(t) = j_T \frac{t}{\tau_R} - \frac{B_o}{2\nu\delta_{ER}^2} \left[i\left(x - \frac{d}{2}\right) + \frac{1}{2d}\left(x^2 - \frac{d^2}{3}\right)\right] \qquad (E-6)$$

for the total current density in the ith conductor as a function of time for a linearly rising magnetic field. The power dissipated in length ℓ of the ith conductor is given by

$$P_i(t) = 2\pi R_{ci} \, \ell \int_0^d (\eta j_i^2) dx \qquad (E-7)$$

$$= 2\pi R_{ci} \eta \ell \int_0^d \left\{j_T \frac{t}{\tau_R} - \frac{B_o}{2\nu\delta_{ER}^2}\right.$$

$$\left.\left[i\left(x - \frac{d}{2}\right) + \frac{1}{2d}\left(x^2 - \frac{d^2}{3}\right)\right]\right\}^2 dx$$

where R_{ci} is the distance from the axis of the multiturn coil to the center of the ith conductor. Squaring and integrating yields:

$$P_i(t) = 2\pi R_{ci} \, \eta \ell \frac{B_o^2}{\nu^2} \left[\frac{1}{(0.4\pi)^2 d} \frac{t^2}{\tau_R^2}\right.$$

$$\left.\frac{d^3}{4\delta_{ER}^4} \left(\frac{1}{45} + \frac{i}{24} + \frac{i^2}{12}\right)\right]. \qquad (E-8)$$

The total power dissipated in ν layers is obtained by summing over i:

$$P(t) = \sum_{i=1}^{\nu} P_i(t). \qquad (E-9)$$

Noting that

$$\sum_{i=1}^{\nu} i = \frac{\nu(\nu + 1)}{2}$$

and $\qquad\qquad\qquad\qquad\qquad$ (E-10)

$$\sum_{i=1}^{\nu} i^2 = \frac{\nu(\nu + 1)(2\nu + 1)}{6}$$

and substituting (E-8) and (E-10) into (E-9), we obtain (for $\nu \gg 1$)

31

$$P(t) = \frac{2\pi \bar{R}_c \, \eta \ell \, B_o^2}{(0.4\pi)^2 \, \nu d} \left[\frac{t^2}{\tau_R^2} + \frac{(0.4\pi)^2 \, \nu^2 d^4}{144 \, \delta_{ER}^4} \right] . \quad (E\text{-}11)$$

The mean radius $\bar{R}_c$ is the radius to the center of the ν-turn coil, i.e., $\bar{R}_c = R_{co} + \frac{\Delta R_c}{2}$, where R_{co} is the inside radius of the coil and ΔR_c is its thickness. From Fig. 17A we see:

$$d = \frac{\lambda}{\nu} \, \Delta R_c \quad (E\text{-}12)$$

$$\epsilon = \left(\frac{1 - \lambda}{\nu - 1} \right) \Delta R_c \quad (E\text{-}13)$$

where d is the thickness of a conducting layer, ϵ is the space for insulation between conducting layers, and λ is the conductor volume fraction. In terms of λ,

$$P(t) = \frac{2\pi \bar{R}_c \, \eta \ell B_o^2}{(0.4\pi)^2 \lambda \Delta R_c} \left[\frac{t^2}{\tau_R^2} + \frac{(0.4\pi)^2 \lambda^2 \Delta R_c^2 d^2}{144 \, \delta_{ER}^4} \right] . \quad (E\text{-}14)$$

To get the total resistive energy losses E_R in the coil during the rising and falling portions of the magnetic waveform we integrate over $0 < t < \tau_R$ and multiply by two:

$$E_R = \frac{2\pi \bar{R}_c \, \eta \ell \, B_o^2 \, \tau_R}{(0.4\pi)^2 \, \lambda \, \Delta R_c} \left[\frac{2}{3} + \frac{\lambda^2 \, \Delta R_c^2 \, d^2}{45.6 \, \delta_{ER}^4} \right]. \quad (E\text{-}15)$$

Of this the amount

$$E_E = \frac{2\pi \bar{R}_c \, \eta \ell \, B_o^2 \, \tau_R}{(0.4\pi)^2 \, \lambda \Delta R_c} \left(\frac{\lambda^2 \Delta R_c^2 d^2}{45.6 \, \delta_{ER}^4} \right) \quad (E\text{-}16)$$

is the eddy current loss. The loss from transport current during the main pulse duration τ is

$$E_T(\tau) = \frac{2\pi \bar{R}_c \, \ell \eta B_o^2 \tau}{(0.4\pi)^2 \, \lambda \Delta R_c} , \quad (E\text{-}17)$$

and the loss from transport current during the rising and falling portions of the waveform is

$$E_T(\tau_R) = \frac{2\pi \bar{R}_c \, \ell \eta B_o^2}{(0.4\pi)^2 \lambda \Delta R_c} \left(\frac{2}{3} \tau_R \right) . \quad (E\text{-}18)$$

The total joule loss in the compression coil during the trapezoidal pulse is given by

$$E_{JC} = E_E + E_T(\tau) + E_T(\tau_R), \quad (E\text{-}19)$$

and the energy loss W_{JC} per unit length is

$$W_{JC} = E_{JC}/\ell . \quad (E\text{-}20)$$

Similarly, the other individual energy losses per unit length are found from $W = E/\ell$.

REFERENCES

1. F. L. Ribe, T. A. Oliphant, Jr., and W. E. Quinn, Los Alamos Scientific Laboratory Report LA-3294-MS (1965).

2. G. I. Bell, W. H. Borkenhagen and F. L. Ribe in Proceedings of the B.N.E.S. Conference on Nuclear Fusion Reactors held at the UKAEA Culham Laboratory 17-19 September, 1969 (UKAEA Culham Laboratory, 1969) p. 242.

3. F. L. Ribe, in Fusion Technology, Proceedings of the Intersociety Energy Conversion Engineering Conference, "Energy 70", Las Vegas, Nevada, USA, 21-25 September 1970, p. 1-13.

4. R. F. Gribble and F. L. Ribe, Los Alamos Scientific Laboratory Report LA-4194-MS (1969).

5. F. L. Ribe, in Los Alamos Scientific Laboratory Report LA-4656-MS, p. 23 (1971).

6. F. L. Ribe, Los Alamos Scientific Laboratory Report LA-4828-MS (1971).

7. T. A. Oliphant in Proceedings of the B.N.E.S. Conference on Nuclear Fusion Reactors held at the UKAEA Culham Laboratory 17-19 September, 1969 (UKAEA Culham Laboratory, 1969) p. 306.

8. F. L. Ribe, Los Alamos Scientific Laboratory Report LA-2471-MS (1960).

9. D. W. Forslund, J. P. Freidberg and R. L. Morse, private communication, 1971.

10. To the author's knowledge this idea was first put forward by R. L. Morse, 1971.

11. K. I. Thomassen, LA-5087-MS and paper presented at the Texas Symposium of the Technology of Controlled Thermonuclear Fusion Experiments and the Engineering Aspects of Fusion, University of Texas at Austin, Nov. 20-22, 1972.

12. P. F. Smith, "Synchrotron Power Supplies Using Superconducting Electrical Storage," Proc. 2nd Int. Conf. on Magnet Technology, Oxford, 1967, p. 589.

13. P. F. Smith and J. D. Lewin, Particle Accelerators, Vol. 1, p. 155, 1970.

14. D. R. Bates, A. E. Kingston, and R. W. P. McWhirter, Proc. Roy. Soc. 267A, 297 (1962).

15. B. Lehnert, Nucl. Fusion 8, 173 (1968).

16. T. A. Oliphant and F. L. Ribe, ANS Transactions, Vol. 15, No. 1, p. 37 (June 1972).

17. S. C. Burnett, W. R. Ellis, T. A. Oliphant, and F. L. Ribe, Los Alamos Scientific Laboratory Report LA-DC-72-234 (1972).

18. S. C. Burnett, W. R. Ellis, and F. L. Ribe, ANS Transactions, Vol. 15, No. 1, p. 36 (June 1972).

19. D. J. Dudziak, paper to be published as a Los Alamos Scientific Laboratory Report (1972).

20. George I. Bell, "Neutron Blanket Calculations for Thermonuclear Reactors," Los Alamos Scientific Laboratory Report LA-3385-MS (1965).

21. George I. Bell, "Neutron Blanket Calculations for Thermonuclear Reactors, II," Los Alamos Scientific Laboratory Report LA-4131-MS (1969).

22. K. D. Lathrop, "DTF-IV, A FORTRAN-IV Program for Solving the Multigroup Transport Equation with Anistropic Scattering," Los Alamos Scientific Laboratory Report LA-3373-MS (1965).

23. Henry C. Honeck, "ENDF/B Specifications for an Evaluated Nuclear Data File for Reactor Applications," Brookhaven Laboratory Report BNL-50066 (1966).

24. G. D. Joanou and J. S. Dudek, "GAM-II: A B_3 Code for Calculation of Slowing Down Spectrum and Associated Multigroup Constants," General Atomics Report GA-4265 (1963).

25. Donald J. Dudziak, "Neutronic Analysis of a CTR Blanket Benchmark by Discrete Ordinates," Trans. Am. Nucl. Soc. 15 (2) (1972).

26. M. A. Abdou and C. W. Maynard, "Neutron Source Geometry Effects on Fusion Reactor Blankets," Trans. Am. Nucl. Soc. 15 (1), 34 (1972).

27. D. Steiner, "The Nuclear Performance of Fusion Reactor Blankets," Nucl. Appl. and Tech., 9, 83 (1970).

28. G. L. Kulcinski, University of Wisconsin, personal communication, July 1972.

29. J. J. Ritts, M. Solomito, and D. Steiner, "Kerma Factors and Secondary Gamma-Ray Sources for Some Elements of Interest in Thermonuclear Blanket Assemblies," Oak Ridge National Laboratory Report ORNL-TM-2564 (1970).

30. W. F. Vogelsang, ANS Transactions, Vol. 15, No. 1, p. 33 (June 1972).

31. H. S. Carslaw and J. C. Jaeger, Conduction of Heat in Solids, (The Clarendon Press, Oxford, 1952), Second Ed.

32. W. V. Green and F. L. Ribe, Los Alamos Scientific Laboratory Report LA-DC-72-125 (1972).

33. S. C. Burnett and W. R. Ellis, Los Alamos Scientific Laboratory Report LA-4814-MS (October, 1971).

34. T. F. Stratton, Temperature-Its Measurement and Control in Science and Industry, Vol. 3, Pt. 1, Reinhold, New York (1962).

35. S. C. Burnett, W. R. Ellis, and F. L. Ribe, Los Alamos Scientific Laboratory Report LA-DC-72-381 (1972).

36. P. J. Persiani, W. C. Lipinski, and A. J. Hatch, paper presented at the Texas Symposium of the Technology of Controlled Thermonuclear Fusion Experiments and the Engineering Aspects of Fusion, University of Texas at Austin, Nov. 20-22, 1972, (Also as Argonne National Laboratory Report ANL-7932, 1972).

37. S. C. Burnett, W. R. Ellis, C. F. Hammer, C. R. Harder, H. W. Harris, F. C. Jahoda, W. E. Quinn, A. S. Rawcliffe, F. L. Ribe, G. A. Sawyer, R. E. Siemon, K. S. Thomas, and E. L. Zimmermann, IAEA Fourth Conference on Plasma Physics and Controlled Nuclear Fusion Research, Madison, Wisconsin (June 1971). Paper CN-28/J-4.

38. W. R. Ellis, C. F. Hammer, F. C. Jahoda, W. E. Quinn, F. L. Ribe, and R. E. Siemon, Proc. Second Topical Conference on Pulsed, High Beta Plasmas, Garching, Munich, W. Germany (July 1972). Paper A-1.

39. F. L. Ribe ed., Los Alamos Scientific Laboratory Report LA-5026-P (September 1972).

ALT:678(440)